https://doi.org/10.1070/RCR5004

Semiconductor photocatalysts and mechanisms of carbon dioxide reduction and nitrogen fixation under UV and visible light

Ekaterina A. Kozlova,[a] Mikhail N. Lyulyukin,[a, b] Denis V. Kozlov,[a, b] Valentin N. Parmon [a, b]

[a] *G.K.Boreskov Institute of Catalysis, Siberian Branch of the Russian Academy of Sciences, prosp. Akademika Lavrentieva 5, 630090 Novosibirsk, Russian Federation,*
[b] *Novosibirsk State University, ul. Pirogova 2, 630090 Novosibirsk, Russian Federation*

The review summarizes the current knowledge about heterogeneous semiconductor photocatalysts that are active towards photocatalytic reduction of carbon dioxide and molecular nitrogen under visible and near-UV light. The main classes of these photocatalysts and characteristic features of their application in the target processes are considered. Primary attention is given to photocatalysts based on titanium dioxide, which have high activity and stability in the carbon dioxide reduction. For the first time, the photofixation of nitrogen under irradiation in the presence of various semiconductor materials is considered in detail.
The bibliography includes 264 references.

Contents

1. Introduction 1520
2. Principle of operation of semiconductor photocatalysts for carbon dioxide reduction 1522
3. Main semiconductor photocatalysts for carbon dioxide reduction 1523
3.1. Titanium dioxide-based photocatalysts 1523
3.1.1. Carbon dioxide reduction catalyzed by unmodified titanium dioxide 1523
3.1.2. Modified titanium dioxide 1525
3.1.2.1. Doping of TiO_2 with metals (nonmetals) 1526
3.1.2.2. Deposition of metals on the titanium dioxide surface 1526
3.1.2.3. Alkaline modification 1526
3.1.2.4. Fabrication of semiconductor heterostructures 1527
3.1.2.5. Modification with carbon materials 1528
3.1.3. Comparison of activities of titanium dioxide-based photocatalysts 1528
3.2. Photocatalysts based on cadmium sulfides 1528
3.3. Photocatalysts based on graphitic carbon nitride g-C_3N_4 1532
3.4. Conclusions about the current state of studies on the photocatalytic reduction of CO_2 1533
4. Reduction of molecular nitrogen in the presence of semiconductor photocatalysts 1534
4.1. Mechanism of nitrogen reduction 1534
4.2. Photocatalytic materials for nitrogen reduction 1535
4.2.1. Metal oxide systems 1535
4.2.2. Metal sulfide systems 1536
4.2.3. Bismuth oxyhalides 1536
4.2.4. Comparative data on the photocatalytic reduction of nitrogen 1537
5. Conclusion 1538
6. List of acronyms and designations 1538

1. Introduction

In the 20th century, energy was mainly produced from fossil fuel.[1, 2] During the last two decades, the consumption of fossil hydrocarbons also considerably increased. A natural consequence of increasing consumption of various sorts of fossil fuel is the appreciable increase in the anthropogenic atmospheric emission of carbon dioxide, resulting from fuel combustion; in the opinion of some experts, this accounts for the global warming taking place in recent years. In 2020, the Energy Strategy of the Russian Federation until 2035 was approved; † among priorities of the Energy Strategy are ... structural diversification, according to which carbon-based energy would be supplemented by non-carbon energy and transition to environmentally benign and resource-saving energy production .

The transition to energy production from renewable energy sources is one of the most efficient approaches to tackle the problem of greenhouse gas emissions. According to forecasts,[3] the share of renewable energy in the global energy consumption should reach 10% by 2040. Other promising ways to decrease the carbon dioxide emission in the atmosphere are to bind CO_2 in the places of its generation and to capture and absorb CO_2 from the atmosphere, as this is done by plants in natural photosynthesis. Thus, binding of CO_2 is relevant not only to the use of carbon dioxide as a source of carbon, *e.g.*, in chemical industry, but also to the decrease in the CO_2 concentration in the atmosphere.

Serious obstacles faced by specialists who develop chemical approaches to binding CO_2 arise from the facts that the linear CO_2 molecule formed upon sp-hybridization of the carbon atomic orbitals is exceptionally thermodynamically stable ($\Delta G^0_{f,\,298} = -394$ kJ mol^{-1}) and relatively inert against reduction. Therefore, the use of carbon dioxide in

† Energy Strategy of the Russian Federation until 2035. Government of the Russian Federation. Order of June 9, 2020, No. 1523-r, Moscow.

Received 27 August 2020

© 2021 Uspekhi Khimii, ZIOC RAS, Russian Academy of Sciences and IOP Publishing Limited

the chemical industry as a potential substrate for the preparation of target products is still very limited. The simplest chemical transformation of CO_2 into much more reactive compound is dissolution in water to give the carbonate anion; the carbon atom in the carbonate anion is more reactive due to sp^2-hybridization. This chemical reaction is of prime importance for the successive transformations that take place during green plant photosynthesis, in which this reaction is accelerated by carbonic anhydrase, a special zinc-containing enzyme.[4] It is quite possible that the development of artificial analogues of carbonic anhydrase may facilitate the absorption of atmospheric CO_2 by natural water bodies, first of all, seas and oceans, which have always been the main natural systems that maintain the CO_2 balance in the atmosphere. However, note that the chemical transformation of CO_2 to the carbonate ion is not accompanied by a change in the valence state of carbon; meanwhile, compounds containing carbon in a lower oxidation state (CO, hydrocarbons, carbohydrates, *etc.*) are more desirable products of CO_2 transformation.

In industry, CO_2 is reduced *via* hydrogenation processes, which take place at rather high temperatures. In living nature, CO_2 is reduced to organic compounds under mild conditions. However, carbon dioxide reduction under chemically mild conditions occurs, as a rule, under the action of additional physical factors such electric field or light radiation. The electrochemical conversion of CO_2 is still at the exploratory stage, which is due to low efficiency and low selectivity of the electrocatalyzed transformations proposed so far (see, for example, Ref. 5). An interesting alternative to electrochemical reactions is the photochemical or photocatalytic conversion of CO_2 to various reduction products,[6] which actually mimic the natural plant photosynthesis. It is known that exposure of the system to UV or visible light eliminates the thermodynamic restrictions on the reductive transformation of carbon dioxide to organic compounds. Possible products of the joint photocatalytic conversion of CO_2 and water are alcohols and hydrocarbons (Fig. 1).

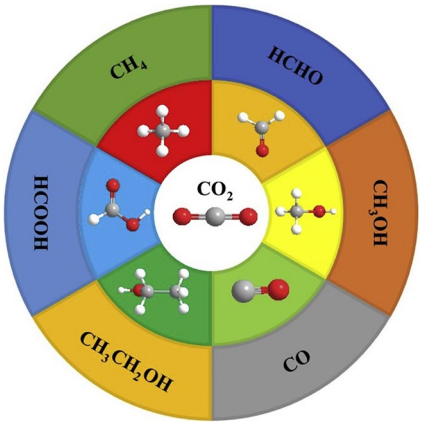


Figure 1. Scheme of CO_2 reduction reactions.[7] Published with permission from Elsevier.

Regarding the environmental protection, large-scale conversion of CO_2 to useful organic products through the energy of sunlight could be the optimal route for solving the problem of disposal of greenhouse CO_2, as in this case, carbon dioxide can be regarded as a renewable raw material source. The most promising approach is the transformation of CO_2 into valuable products using the sunlight as an inexhaustible energy source. However, since the use of light emitting diodes and other unconventional light sources appreciably increases the efficiency of conversion of electrical energy to light energy, the photochemical transformations of CO_2 under the action of artificial light sources are also of obvious interest.

The light-stimulated CO_2 conversion to useful products in artificial systems is a subject of studies, the activity of which has markedly increased over the last 10–15 years.[1,7–13] The greatest attention has been devoted to the photocatalytic reduction of carbon dioxide, which results in the formation of simple organic compounds such as formaldehyde, methane and methanol.[14]

In the case of photocatalytic reduction of carbon dioxide, the photocatalyst performs three functions:[15,16] (1) absorbs light; (2) ensures spatial separation of photogenerated charge carriers; and (3) gives rise to surface active sites for dark catalytic reactions.

The heterogeneous photocatalytic systems based on TiO_2 or ZnS type semiconductors have been studied in most detail. These materials are responsible for all the three above-mentioned functions, although in some cases, they are used together with sensitizers, which enhance the visible light absorption. The dark chemical step usually proceeds most efficiently on the surface of a co-catalyst, but can also take place on the semiconductor surface. The co-catalysts used most often are metals (Pt, Pd, Cu, Ni, *etc.*) or metal oxides (NiO, RuO_2), which form composite structures with the semiconductor and ensure the spatial separation of photogenerated charge carriers.

The photocatalytic reduction of CO_2 is a multielectron process, which may give various compounds depending on the particular reaction pathway. A variety of products have been identified in experiments, mainly carbon monoxide and light hydrocarbons;[17] however, in some cases, the formation of oxalic acid, acetaldehyde, ethanol and higher hydrocarbons and alcohols was detected. It is evident that the photocatalytic CO_2 reduction is an intricate and nonselective process; therefore, it is necessary to understand the

E.A.Kozlova. Doctor of Chemistry, Leading Researcher at IC SB RAS.
E-mail: kozlova@catalysis.ru
Current research interests: semiconductor photocatalysis for hydrogen production and destruction of harmful organic substances.
M.N.Lyulyukin. Candidate of Chemical Sciences, Researcher at IC SB RAS, Assistant at the Department of General Chemistry and the Department of Physical Chemistry, Faculty of Natural Sciences, NSU.
E-mail: lyulyukin@catalysis.ru
Current research interests: development and study of semiconductor photocatalytic systems sensitive in a wide spectral range for oxidative destruction of harmful organic impurities and carbon dioxide photofixation.
D.V.Kozlov. Doctor of Chemistry, Professor of RAS, Head of the Department of Unconventional Catalytic Processes, IC SB RAS, Director of the Research and Education Centre Institute of Chemical Engineering.
E-mail: kdv@catalysis.ru
Current research interests: photo and electrocatalytic processes for alternative energy, environmental protection and sustainable development.
V.N.Parmon. Academician, Doctor of Chemistry, Chairman of SB RAS, Scientific Director of IC SB RAS, Professor and Head of the Department of Physical Chemistry, Faculty of Natural Sciences, NSU.
E-mail: parmon@catalysis.ru
Current research interests: development and study of catalysts and catalytic processes, particularly for the conversion and storage of various kinds of energy, catalysis and photocatalysis in nature and in the use of renewable and non-traditional energy resources.

Translation: Z.P.Svitanko

reaction mechanism in order to establish conditions for selective reduction.

In particular, high concentration of CO_2 on the photocatalyst surface is an important factor; this is especially important for the reduction of carbon dioxide with water. In air, the CO_2 to H_2O molar ratio is 1 : 1300 at a pressure of 1 atm.[18] In addition, the entry of CO_2 molecules to the photocatalyst surface is limited by their slow diffusion.[19] Correspondingly, it is necessary to reduce the concentration of protons and increase the concentration of CO_2 on the photocatalyst surface, for instance, by using photocatalysts with a hydrophobic surface.[20] Also, it is beyond doubt that the activity and selectivity of photocatalytic reduction of carbon dioxide is considerably influenced by hydrophilicity or hydrophobicity of the photocatalyst surface.[21]

An interesting issue is the light-induced fixation of readily available, but very inert molecular nitrogen, which proceeds under UV or visible light irradiation. The photocatalytic reduction of nitrogen has been little studied in comparison with the reduction of carbon dioxide, although the basic features of the action of semiconductor catalysts in these processes are quite similar.[22]

The main factors hampering the development of methods for the photocatalytic reduction of carbon dioxide and nitrogen are the deficiency of data on suitable efficient and stable heterogeneous photocatalysts and the lack of unambiguous understanding of factors that determine the selectivity of these processes.[23] In view of the foregoing, this review addresses some aspects of the mechanisms of carbon dioxide and nitrogen reduction and the main classes of photocatalysts suitable for these reactions.

2. Principle of operation of semiconductor photocatalysts for carbon dioxide reduction

The first step of the photocatalytic process using semiconductors includes absorption of light quanta by the semiconductor and gives rise to photogenerated electrons (e^-) and holes (h^+) in the conduction band (CB) and valence band (VB) of the semiconductor. The electrons and holes have strong reducing and oxidizing properties, respectively. They can migrate to the semiconductor surface and subsequently participate in redox processes.

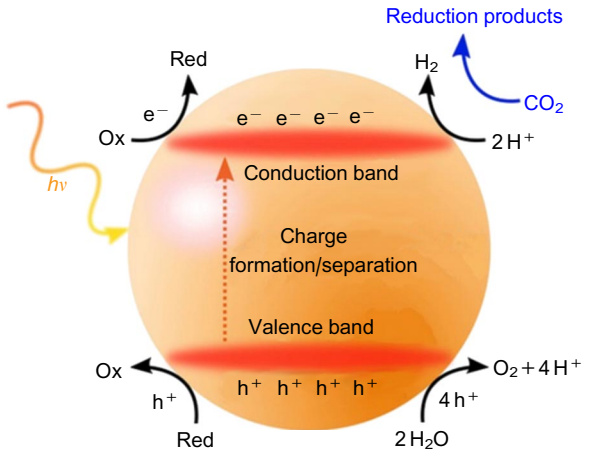


Figure 2. Formation of photogenerated electron–hole pairs and redox reactions involving these pairs, including the reactions of CO_2 and H_2O.[1] Published with permission from Wiley.

Thus, the key factors affecting the photocatalytic activity of a semiconductor material are (1) the ability of the photocatalyst to absorb light; (2) electron–hole separation efficiency; (3) the ability of components of the material to catalyze a particular transformation on the surface (Fig. 2).

The reduction of water to give hydrogen and the reduction of CO_2 to give CO and organic compounds require relatively strong reducing agents, which can be represented by photogenerated electrons. Despite the fact that the possibility of photocatalytic implementation of both processes was established back in the 1970s, currently the photocatalytic reduction of CO_2 has been markedly less studied that the reduction of water to give hydrogen.[24,25]

The complexity of the photocatalytic reduction of the CO_2 molecule is primarily related to high energy required for C=O bond cleavage. The single-electron reduction of CO_2 to the $CO_2^{-\bullet}$ radical anion requires a reducing agent with a great negative potential [more negative than −1.9 V *vs.* the normal hydrogen electrode (NHE) at pH 7]. None of known semiconductors with a rather narrow band gap has a sufficiently great negative CB level. The simultaneous multielectron oxidation of water requires that the valence band top be more positive than 0.81 V *vs.* NHE at pH 7. Meanwhile, the multielectron reduction of CO_2 involving protons requires less negative electrochemical potentials of the reducing agent. Table 1 summarizes the standard electrode potentials *vs.* NHE at pH 7 for the most probable carbon dioxide reduction reactions.[26]

The reduction of CO_2 to valuable products includes the carbon hydrogenation and, in some cases, carbon–carbon bond formation steps. For multielectron reduction of carbon dioxide to occur, it is necessary to overcome not only thermodynamic, but also kinetic restrictions. It is noteworthy that CO_2 is sparingly soluble in water (0.8–1.0 vol.% at 20 °C and a CO_2 pressure of 1 bar). In addition, the CO_2 adsorption capacity of most semiconductor photocatalysts is moderate. As a result, the concentration of CO_2 on the photocatalyst surface where the active sites are located is very low, which accounts for low efficiency of the carbon dioxide reduction.

It is evident that photocatalytic water decomposition and carbon dioxide reduction include the following similar steps: light absorption by the photocatalyst, formation of electron–hole pairs and migration of the photogenerated charge carriers to the photocatalyst surface. These two processes differ in the reactions involving conduction electrons on the catalyst surface: hydrogen is formed *via* the reduction of protons followed by recombination of hydrogen atoms, while the reduction of CO_2 follows a more complex mechanism, which includes CO_2 adsorption and

Table 1. Standard electrode potentials (E^0) *vs.* NHE at pH 7 for the most probable reactions involving water and carbon dioxide (according to Morris *et al.*[26]).

Reaction	E^0, V, *vs.* NHE
$2H_2O + 4h^+ \rightarrow 4H^+ + O_2$	+0.81
$2H^+ + 2e^- \rightarrow H_2$	−0.42
$CO_2 + e^- \rightarrow CO_2^{-\bullet}$	−1.90
$CO_2 + 2H^+ + 2e^- \rightarrow HCO_2H$	−0.61
$CO_2 + 2H^+ + 2e^- \rightarrow CO + H_2O$	−0.53
$CO_2 + 4H^+ + 4e^- \rightarrow HCHO + H_2O$	−0.48
$CO_2 + 6H^+ + 6e^- \rightarrow CH_3OH + H_2O$	−0.38
$CO_2 + 8H^+ + 8e^- \rightarrow CH_4 + 2H_2O$	−0.24

activation and formation of products *via* successive steps of C=O bond dissociation and C–H (and probably C–C) bond formation on the surface of the photocatalyst. The reduction of carbon dioxide in both gas and liquid phases may yield a large number of products, which is still an obstacle hampering elucidation of the actual reaction mechanism.[1] The vast majority of studies dealing with the photocatalytic reduction of CO_2 are aimed at the synthesis of new photocatalysts, and only a minor portion of studies address the reaction mechanism. One more obstacle hampering the experimental study of the photocatalytic reduction of CO_2 is the possibility that detectable carbon-containing products may result from photoinduced reactions with carbon compounds usually present in residual amounts on the semiconductor surface, but not from the CO_2 reduction.

Nevertheless, in one of the most comprehensive studies[27] of the photocatalytic reduction of carbon dioxide in the presence of TiO_2, it was shown using ^{13}C isotopes and mass spectroscopy that if the gaseous reaction mixture consists of only CO_2 and water, carbon present in the obtained organic compounds comes exactly from CO_2 rather than from the residual carbon-containing impurities present in the photocatalyst.[27] The nature of the sacrificial reducing agent is varied rather rarely; most often, water is used for this purpose, although in this case, the side reaction of photocatalytic formation of hydrogen proceeds in parallel.[28] A relatively small number of publications are devoted to the design of photocatalytic reactors and investigation of the effect of photocatalyst irradiation conditions on the yield and composition of the CO_2 photoreduction products (see, *e.g.*, Ref. 24). In most studies describing the mechanism of the photocatalytic reduction of CO_2, contradictory and sometimes even mutually exclusive conclusions are drawn. Therefore, for systematic studies of this reaction, it is necessary to monitor the conditions of the gas phase and the state of the catalyst surface and to conduct experiments using isotopes.

3. Main semiconductor photocatalysts for carbon dioxide reduction

The search for active heterogeneous photocatalysts for the reduction of carbon dioxide have been actively carried out since 1979 starting with the pioneering study of Inoue *et al.*[25] on the photocatalytic reduction of carbon dioxide in suspensions in the presence of a large set of typical semiconductor photocatalysts (TiO_2, CdS, WO_3, ZnO, *etc.*). In recent years, numerous materials have been tested as photocatalysts for this reaction, including oxides ZrO_2,[30,31] MgO,[32] Ga_2O_3,[33] $ATaO_3$ (A = Li, Na, K), CaO and Al_2O_3 [32,34] and sulfides such as ZnS (Ref. 35) and Bi_2S_3.[36] A lot of attention was given to photocatalysts for carbon dioxide reduction based on graphitic carbon nitride — g-C_3N_4.[37–42]

Below, various groups of materials tested as photocatalysts for the reduction of carbon dioxide are considered in detail.

3.1. Titanium dioxide-based photocatalysts

Cheap and non-toxic titanium dioxide is used most often as a semiconductor photocatalyst for CO_2 reduction.[16,43,44] The major drawback of this catalyst is that pure (unmodified) TiO_2 is insensitive to visible light, because the band gap of this oxide is 3.2 eV.[28] Therefore, the performance of titanium dioxide on exposure to sunlight is insufficient.

One more drawback of pure TiO_2 is relatively fast recombination of photogenerated electron–hole pairs and, as a consequence, low quantum efficiency of the target photocatalytic process.[45] The quantum efficiency of TiO_2-initiated photocatalytic reactions can be markedly increased by the spatial separation of photogenerated charges (electrons and holes). A promising way to reach this goal is to produce composite semiconductor materials,[46] *e.g.*, structures with interfacial heterojunctions for photogenerated charges.[47]

The band structure of TiO_2 is mainly favourable for the light-induced oxidation rather than for reduction reactions, which require a negative electrode potential of photogenerated electrons. Therefore, the main trend of the studies on the photocatalytic fixation of CO_2 is modification of the band structure of titanium dioxide. Below we consider the known approaches to the use of pure, modified and doped TiO_2 and describe the results on the light-induced carbon dioxide reduction with several photocatalytic systems and the main regularities of the studied processes.

3.1.1. Carbon dioxide reduction catalyzed by unmodified titanium dioxide

Titanium dioxide readily adsorbs diverse organic compounds and can contain their residual amounts of these compounds that have got there during the synthesis. Since such compounds can also undergo photoinduced reactions during CO_2 reduction, it is highly important to identify the real source of carbon in the detectable products of the light-induced process. For example, illumination of TiO_2 in an oxygen-free atmosphere may result in the formation of methane from adsorbed organic compounds. By using isotopically labelled $^{13}CO_2$, it was shown that irradiation of TiO_2 synthesized from titanium isopropoxide gives methane containing no ^{13}C isotope; hence, methane is not a product of carbon dioxide reduction, but is formed from the organic precursor that got into TiO_2 during the preparation of the photocatalyst.[48]

Relatively high yields of the products of CO_2 reduction catalyzed by TiO_2 were observed for systems that contained H_2 and saturated water vapor, apart from carbon dioxide.[49] In this case, the formation of CO, CH_4 and C_2H_6 was detected under UV irradiation. The quantum efficiency of the transformation of CO_2 was ~7%. The authors simulated the photoreduction of CO_2 using the Langmuir–Hinshelwood model. The possibility of describing the kinetics of CO_2 photoreduction in terms of this model was also demonstrated by Ku *et al.*,[50] who studied the reduction of carbonate anions dissolved in water on exposure to UV radiation in the presence of suspended TiO_2 Degussa P25. The major reduction products were methanol and methane. It was shown that the photocatalytic reduction of carbonate anions proceeds more efficiently in an acid medium and that the reaction rate linearly depends on the light intensity and is proportional to the concentration of TiO_2 in the suspension.

Some studies are devoted to the effect of the structure and phase composition of titanium dioxide on its activity towards the photocatalytic reduction of CO_2. For example, Chen *et al.*[51] used magnetron sputtering of titanium for the synthesis of TiO_2 films with a mixed phase composition on borosilicate glasses. Characteristics of a series of films that were obtained by sputtering at different deposition angles and had different phase compositions were compared with characteristics of the TiO_2 P25 film by testing in CO_2

photoreduction induced by UV and visible light. A film based on 70% anatase and 30% rutile obtained at a low deposition angle proved to be more efficient as regards the initial reaction rate and the degree of conversion of CO_2 to methane. At an elevated temperature and a high CO_2 concentration, the degree of conversion of CO_2 to methane attained in a four-hour experiment was ~12%.

A standard reference material in photocatalysis is highly active titanium dioxide P25 (Evonik, formerly Degussa): a composite TiO_2 powder made of ~80% anatase and 20% rutile with a specific surface area of 40 to 60 $m^2 g^{-1}$ (Ref. 52) and particle diameter of 20 to 80 nm (on average, ~25 nm). Thus, the greatest number of studies of carbon dioxide reduction have been carried out using particularly P25 titanium dioxide.[53–57]

The high activity of P25 is attributed to interaction between the two phases that make up the material that is, anatase and rutile,[58,59] with phase interfaces being considered to be most important.[60,61] Indeed, CB of anatase is located ~0.2 eV higher than CB of rutile, which gives rise to a heterojunction. For photogenerated electrons, it is energetically more favourable to migrate from anatase to rutile, while the generated holes remain in anatase, thus providing spatial separation of the photogenerated charges. However, this model is not generally recognized.[54] An alternative explanation of the high photocatalytic activity is provided by the presence of electron traps in anatase, which are located 0.8 eV below the conduction band edge.[62]

In most studies, irradiation was performed by mercury lamps, the main peaks in the emission spectrum of which are located in the UV region. Both near-UV (UV-A) and far-UV (UV-C) lamps were used for the photoreduction of CO_2 in the presence of titanium dioxide. It was shown[63] that under these irradiation conditions, CO_2 can be converted to methane on contact with water.

Analysis of the possible pathways of the photoinduced reduction of CO_2 to methane catalyzed by titanium dioxide was reported by Habisreutinger *et al.*[15] The CO_2 activation proceeds *via* single-electron formation of surface-bound $CO_2^{-\bullet}$; the subsequent reduction is continued *via* a number of elementary steps, including the transfer of electron, proton or hydrogen radical ($H^\bullet$), cleavage of C–O bonds and formation of new C–H bonds. Although the sequence of steps and details of each step have not yet been fully clarified, three possible pathways for CO_2 conversion to methane have been proposed. These pathways are named according to the nature of intermediates involved in the sequence of CO_2 transformations (Fig. 3): (1) formaldehyde; (2) carbene and (3) glyoxal pathways.

The deviations between the reaction pathways start from the formation of the surface-bound $CO_2^{-\bullet}$ radical anion. The monodentate binding *via* one oxygen atom of this radical anion to a titanium cation or binding *via* the carbon atom to the surface bridging oxygen usually favours the formation of the carboxyl radicals $^\bullet$COOH.[64] Conversely, the bidentate binding *via* both oxygen atoms of the $CO_2^{-\bullet}$ radical anion promotes the addition of the hydrogen atom to the carbon atom to give a formate anion bound in the bidentate fashion.[65] The proton reduction with a photogenerated electron that appears in the conduction band also gives rise to a free hydrogen atom (radical) (see Fig. 3).

According to the formaldehyde mechanism (*1*), the $CO_2^{-\bullet}$ carboxyl radical anion recombines with the hydrogen atom to give formic acid.[66] This pathway is most probable in a liquid medium with a high dielectric constant, for

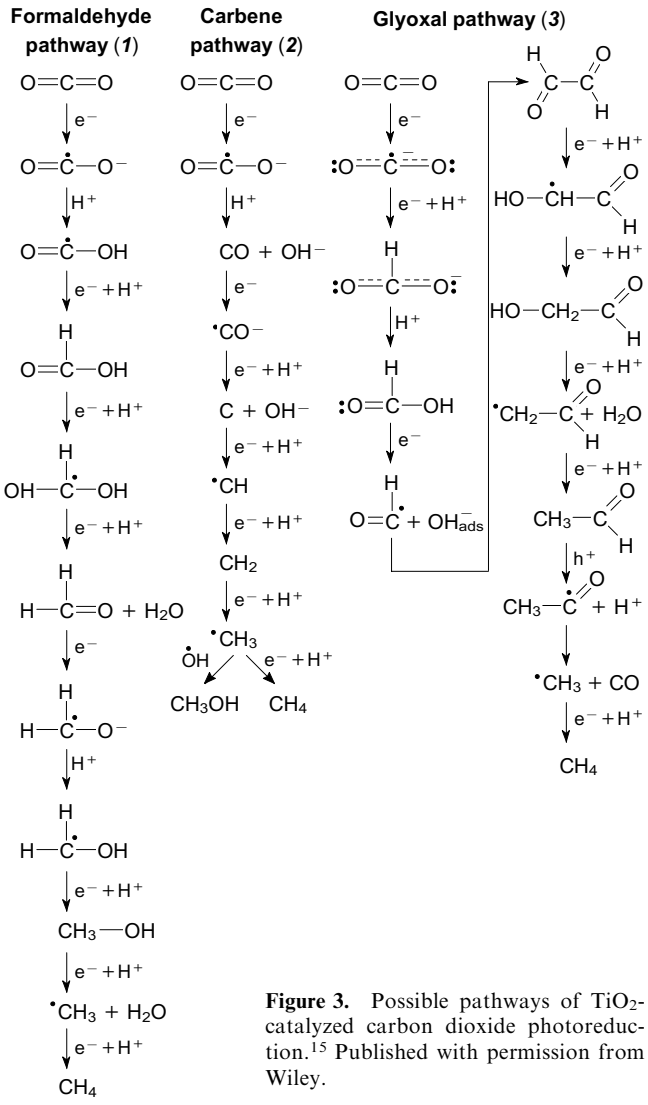


Figure 3. Possible pathways of TiO_2-catalyzed carbon dioxide photoreduction.[15] Published with permission from Wiley.

example, in water. In the next step, formic acid accepts an additional hydrogen atom, being converted to a dihydroxymethyl radical, which loses a water molecule upon the addition of one more $H^\bullet$ to give formaldehyde. The two subsequent reduction steps result in the formation of methanol, which is then reduced *via* two more steps to give methane. The discussed mechanism has two important features. First, formaldehyde and methanol are formed as chemisorbed intermediates and are not released to the bulk as by-products. Second, C–O bond cleavage in this reaction takes place only in the last-but-one step. It is noteworthy that mechanism *1* has not yet received an adequate experimental evidence. In some experiments, the formation of formaldehyde and methanol were observed; however, some specific intermediate steps involving radicals have not yet been confirmed. If this pathway is actually implemented, one should expect accumulation of, for example, methanol before the formation of methane; however, this has not been confirmed experimentally. Moreover, in some studies, data on the photocatalytic reduction of CO_2 were juxtaposed with the kinetic model of the formaldehyde pathway; the results showed incomplete correlation of the kinetic profiles of methane and methanol formation with the proposed mechanism.

According to the carbene pathway (*2*), the addition of the hydrogen radical to the oxygen atom of the adsorbed $CO_2^{-\bullet}$ radical induces immediate elimination of one oxygen atom to give the OH^- anion.[67] This mechanism is most likely if $CO_2^{-\bullet}$ is attached to the semiconductor surface through the radical anion carbon. The CO molecule remains adsorbed and can accept two more electrons; this should give rise to carbon atoms on the surface, which is confirmed by EPR spectroscopy.[67] After that, carbon atoms can be combined with four hydrogen atoms to successively give the $CH^{\bullet}$ radical, carbene, methyl radical or (upon saturation) methane. The recombination of the methyl radical with the hydroxyl radical gives methanol. This means that methanol is a side rather than intermediate product in this pathway, while formaldehyde is not formed at all. Note that CO, methane and methanol were detected in most experiments on the photocatalytic CO_2 reduction.[68, 69]

Ikeue and co-workers.[21,70] described the competing formation of methanol and methane from the methyl radical; the probability of appearance of a particular product depends on the surface hydrophilicity of the semiconductor and water concentration in the system. It is worth noting that the experimental data on the accumulation of methanol and methane are in much better agreement with the kinetic model of mechanism (*2*),[71] indicating that the carbene pathway is more likely than the formaldehyde one.

Shkrob *et al.*[72, 73] identified the intermediate products of CO_2 reduction in an aqueous suspension of TiO_2 nanoparticles (anatase) by EPR spectroscopy. Of particular interest was the revealed proneness of the species resulting from $COO_2^{-\bullet}$ redution (formic acid, formaldehyde and methanol) to participate in the reduction reactions rather than in possible oxidation reactions in the presence of photogenerated holes. The involvement of titanium dioxide and some other semiconductor photocatalysts in oxidation reactions is an important aspect because of their high oxidative capacity under the action of light.

The $CO_2^{-\bullet}$ radical anion bound to the TiO_2 surface in the bidentate fashion is able to add a hydrogen atom to give a C–H bond and, hence, formate anion. This transformation occurs so rapidly that the intermediate cannot be detected by EPR. Then the bidentate formate adds a proton to form a formic acid molecule adsorbed in the monodentate fashion. However, formic acid is rather easily oxidized to give the monodentate $CO_2^{-\bullet}$ radical anion, which is bound more strongly. Shkrob *et al.*[73] concluded that the only pathway possible for CO_2 reduction involving formic acid as an intermediate is a concerted reaction in which the electron transfer from the TiO_2 conduction band to an acid molecule is conjugated with dissociation of the acid and formation of a bond between the hydroxyl oxygen and a titanium cation in the TiO_2 surface layer. It is noteworthy that the energy of Ti–O bond formation exceeds the energy required for the electron transfer during the CO_2 reduction.[73] This transformation gives rise to the $HC^{\bullet}O$ free radical, which can be detected by EPR. The possibility of intermediate formation of this species was also confirmed by other researchers.[74]

In addition, it was found that formaldehyde and methanol are more readily oxidized than reduced under the same experimental conditions.[73] This led to the conclusion that the reduction of CO_2 to CH_4 is not accompanied by the formation of formaldehyde and methanol as intermediates, and an alternative mechanism was proposed, which included, in particular, recombination (dimerization) of formyl radicals to give glyoxal (oxalaldehyde). This compound has a significant electron affinity; therefore, it is easily reduced to glycolaldehyde [CH_2(OH)CHO]. The subsequent sequence of transformations leads to acetaldehyde *via* the formation of experimentally confirmed intermediates. Acetaldehyde is oxidized to an unstable acetyl radical and can be converted to a methyl radical and carbon monoxide. Carbon monoxide is a frequently observed product of CO_2 reduction. Methyl radicals can be produced either from acetaldehyde or by a different pathway: if acetaldehyde is oxidized to acetic acid, the latter is decarboxylated to give a methyl radical and a CO_2 molecule, which is able to start the sequence of transformations once again. In addition, Shkrob *et al.*[73] considered the possible formation of some other intermediate C_2 compounds such as oxalic, glyoxylic and glycolic acids. However, they cannot serve as sources of methyl radicals due to the susceptibility to oxidation.

The complex pathway of CO_2 reduction described above makes it possible to avoid the intermediate stages that suppress the conversion of CO_2 to methane. Meanwhile, the alternation of reduction and oxidation steps, as well as involvement of the mechanism of CO_2 recycling can partially account for the low photon efficiency of the photoreduction of CO_2 in the presence of TiO_2. Thus, the hypothesis of the glyoxal pathway of CO_2 conversion seems to be important for the understanding of the complex mechanism of the photocatalytic CO_2 reduction catalyzed by titanium oxide systems.

During long-term photocatalytic experiments on CO_2 reduction in closed systems, organic compounds more complex than methane or methanol can be formed (see, for example, Ref. 75). However, low rates of accumulation of such products and low photon efficiencies of these reactions preclude the possibility of practical significance of this route.

The requirements for the potential practical applicability of semiconductor photocatalysts in redox catalytic processes are well known:[76]

1. the electrochemical potential of a photogenerated hole should be sufficiently positive to enable the hole to accept an electron from accessible electron donors;

2. the electrochemical potential of a photogenerated electron should be sufficiently negative for the reduction of the target substrate;

3. the photocatalyst material should be stable to photocorrosion and should not generate toxic by-products;

4. the photocatalyst material should be readily available and its use should be economically feasible.

Titanium dioxide is quite consistent with the first, third and fourth requirements. However, the bottom of the conduction band and, hence, the electrochemical potential of a photogenerated electron located in this band are insufficiently negative for conducting the CO_2 reduction under normal conditions. This necessitated the search for systems based on modified TiO_2 for photocatalytic CO_2 reduction.

3.1.2. Modified titanium dioxide

Currently, there are five fundamentally different approaches to the modification of titanium dioxide. These approaches are considered below, together with the results of experiments on the photocatalytic reduction of CO_2 using modified TiO_2.

3.1.2.1. Doping of TiO_2 with metals (nonmetals)

The relatively large band gap of TiO_2 ($\sim$3.2 eV for anatase) restricts the possibility of using sunlight for photocatalytic processes (see above). The expansion of the optical absorption of TiO_2 to the visible region makes it possible to utilize a markedly larger part of the emission spectrum for initiating the reactions, because up to 45% of solar energy is in the visible region.[77–79]

Doping is one of the most common approaches to expansion of the optical absorption range of semiconductors by decreasing the band gap.[80–85] Historically, doping with metals and nonmetals has been commonly considered separately.[86–89] The atoms of many metals such as Cu or In can replace titanium atoms in the crystal lattice of the dioxide and generate unoccupied energy levels below the bottom of the conduction band of pure TiO_2. The appearance of new accessible energy levels increases the efficiency of light absorption and, hence, expands the possibility of using the energy of the incident photons for carrying out the target reaction. For example, doping of titanium dioxide with copper using a modified impregnation method noticeably improves the photocatalytic properties of TiO_2 towards the CO_2 photofixation; as was to be expected, the yield of methanol noticeably increased with increasing quantity of the introduced copper atoms.[90] Nevertheless, it is significant that excessive doping leads to an increase in the defectiveness of the semiconductor structure and, as a consequence, to suppression of the photocatalytic activity of the system due to acceleration of recombination of the photogenerated charge carriers.

Apart from the mentioned metals, La,[91] In,[92] Co (Ref. 85) and some other metals were tested as dopants for TiO_2. A beneficial photocatalytic effect of metal doping of titanium dioxide was repeatedly confirmed; however, the application of this modified TiO_2 is limited by increasing photocorrosion, which hampers the application of photocatalytic systems with a liquid phase.[93,94] Therefore, considerable attention is paid to doping of TiO_2 with nonmetals (*e.g.*, iodine, nitrogen, sulfur or carbon compounds), which replace oxygen when incorporated in the TiO_2 structure.[95–98] In this case, narrowing down of the band gap is attained by inclusion of already occupied energy levels, which lift the valence band top. Particular interest is aroused by doping with nitrogen, which is successfully used for modification of both bulk titanium dioxide both and TiO_2 nanotubes.[99,100] Nitrogen doping of TiO_2 not only enhances the light absorption, but also allows for the control of the selectivity of the photocatalytic CO_2 reduction.

3.1.2.2. Deposition of metals on the titanium dioxide surface

It was indicated above that high probability of the undesirable recombination of photogenerated charge carriers (electrons and holes), in particular on the semiconductor surface, is one of the causes for low efficiency of titanium dioxide for the photocatalytic fixation of CO_2.[101–103] The most widely used approach to address this challenge is the formation of traps for photogenerated electrons on the titanium dioxide surface by deposition of metal nanoparticles, which serve simultaneously as catalysts of dark reactions. The deposition of highly dispersed Pt, Au, Ag or Pd is used most often to improve the photocatalytic characteristics of systems. The Fermi level of these metals is located below the bottom of titanium dioxide conduction band; therefore, the photogenerated electron falls down from the conduction band over the Schottky barrier onto the metal nanoparticle, whereas the photogenerated hole remains on titanium dioxide. This results in spatial separation of photogenerated charge carriers and significantly increases their lifetime and the probability of participation in the target dark reaction. A significant factor for the photogenerated charge separation is the electron work function of the deposited metal (the difference between the work functions of the metal and the semiconductor): the larger this value, the higher the Schottky barrier and, hence, the more restrained the recombination of photogenerated electrons with holes.

One of the highest electron work functions (5.1–5.9 eV) is inherent in Pt metal,[104,105] which is used most often to increase the quantum efficiency of the photocatalytic reduction of CO_2.[106,107] The stability and reproducibility of the results made it possible to study the dependence of the activity of CO_2 reduction photocatalysts on the size of platinum nanoparticles.[108]

In order to utilize the unique surface plasmon resonance phenomenon for expanding the range of action of TiO_2 to the visible region, deposition of, *e.g.*, Ag and Au nanoparticles is carried out.[109–114] This phenomenon occurs when the frequency of the incident radiation coincides with the frequency of natural oscillations of free electrons in the metal nanoparticle on the catalyst surface; in this case, hot electrons may appear on the surface and, owing to their high energy, they migrate to the semiconductor and initiate photocatalytic reactions. Since the light absorption frequencies for the surface plasmon resonance of Au and Ag are located in the visible region, deposition of the nanoparticles of these metals on the TiO_2 surface sensitizes titanium dioxide towards photocatalytic CO_2 reduction on exposure to visible light.[115]

The interaction with plasmon metals can endow titanium dioxide with conceptually new properties if core–shell structures,[116,117] double-shelled hollow spheres [118] or other ordered three-dimensional structures are created (Fig. 4).[119] These structures ensure more efficient absorption of incident light and efficient separation of photogenerated charge carriers, which has a noticeable effect on the photocatalytic activity of these systems towards CO_2 reduction.

3.1.2.3. Alkaline modification

An important stage of the photocatalytic process is adsorption of compounds participating in the chemical reaction on the photocatalyst: more efficient adsorption leads to more

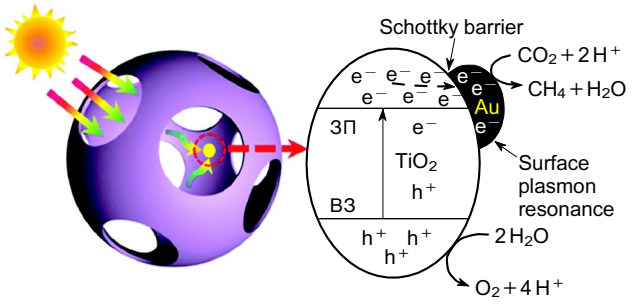


Figure 4. Schematic view of the photocatalytic reduction of CO_2 on nanostructured titanium dioxide with deposited gold according to Jiao *et al.*[119] CB is conduction band, VB is valence band. Published with permission from AIP Publishing.

efficient reaction.[120, 121] Since CO_2 has acidic properties, alkaline modification of the titanium dioxide surface is beneficial for CO_2 adsorption. Moreover, with such modification, CO_2 molecules are involved in the surface chemical transformations, which promote their activation towards the subsequent reactions.

It was shown [122] that treatment of the TiO_2 surface with an alkali (NaOH) using impregnation followed by calcination markedly increases the yield of methane upon the photocatalytic CO_2 reduction in the gas phase. However, this treatment can reduce the specific surface area, and, hence, the overall activity of the photocatalyst due to the possible aggregation of TiO_2 particles. The deposition of magnesium oxide on titanium dioxide increases the rate of CO_2 reduction in the presence of water vapour.[123]

In industry, CO_2 is often captured with compounds containing amino groups. Therefore, it is not surprising that modification of the TiO_2 surface with appropriate amines also leads to good results.[124 – 126]

3.1.2.4. Fabrication of semiconductor heterostructures

The fabrication of composites in which TiO_2 contacts with semiconductor materials of a different nature may provide a better spatial separation of photogenerated electron – hole pairs and the oxidative and reductive active sites of the photocatalysts. This markedly enhances the efficiency of the photocatalytic CO_2 reduction.[127] In the general case, semiconductor heterostructures can be conventionally split into four categories according to the mechanism of separation of photogenerated charges: so-called type II heterojunction,[128 – 130] p – n junction,[131 – 135] direct Z scheme [136 – 142] and surface heterojunction.[143, 144] In this review, we do not consider the fundamentals of formation of these heterojunctions or the nature of their functioning, because they have been described in sufficient detail for a broad range of catalytic processes.[145 – 152]

An efficient way of sensitizing titanium dioxide is to fabricate composite systems in which TiO_2 is in contact with the semiconductor that absorbs visible light, *e.g.*, cadmium sulfide.[153] The $CdS - TiO_2$ systems showed activity towards the photocatalytic reduction of carbon dioxide in the presence of water vapour to give carbon monoxide,[154] methanol [155] and methane [156] on irradiation with visible light at a > 400 nm wavelength.

Table 2. Data in the photocatalytic reduction of CO_2 in the presence of photocatalysts based on TiO_2.

Photocatalyst	Light source, electric power, irradiation conditions	Medium, conditions	Product, rate, $\mu mol\, g^{-1}\, h^{-1}$	Φ (%) (see [a])	Ref.
TiO_2	Four low-pressure mercury lamps, 15 W, unfiltered	GP [b] (CO_2 5%; H_2 90%; 5% H_2O with a total pressure of 1 bar)	CH_4, 4.11 CO, 0.14 C_2H_6, 0.10	–	49
2.5% Ag/TiO_2	Xenon lamp, 500 W, filter > 420 nm	Aqueous suspension of the photocatalyst; CO_2 (1 bar)	CH_3OH (UV + Vis), 405 CH_3OH (Vis), 90	0.5	160
Pt/Ag-TiO_2	Xenon lamp, 350 W, unfiltered	Aqueous suspension of the photocatalyst; CO_2 (4 bar)	CH_4, 160 H_2, 88 O_2, 395	–	161
Au/CdS/TiO_2	Xenon lamp, 300 W, filter 320 – 780 nm	Aqueous suspension of the photocatalyst; CO_2 (1 bar)	CH_4, 41.6 CO, 0.6	~ 0.002	162
2% Cu/TiO_2	Mercury lamp, 8 W, 254 nm	Suspension in 0.2 M NaOH, CO_2 (1 bar)	CH_3OH, ~ 40	–	163
1% Cu/TiO_2	Mercury lamp, 8 W, 254 nm	GP; CO_2 (1 bar)	CO, 334	–	164
La_2O_3/TiO_2	Xenon lamp, 300 W, unfiltered	GP; CO_2 (1 bar)	CH_4, 3.5 CO, 0.5	~ 0.01	91
In/TiO_2	Mercury lamp, 500 W, 365 nm	GP; CO_2 (1 bar)	CH_4, 244 CO, 81.2	~ 3	92
Co/TiO_2	Xenon lamp, 300 W, unfiltered	Aqueous suspension of the photocatalyst; CO_2 (0.8 bar)	CH_4, 0.015 – 0.180 CO, 0.23 – 1.94	–	85
TiO_2 P25	Xenon lamp, 300 W; filter > 420 nm	GP; CO_2 (1 bar)	CH_4, 1.1	–	119
3D TiO_2 structure	Xenon lamp, 300 W; filter > 420 nm	GP; CO_2 (1 bar)	CH_4, 1.4	–	119
Au/3D TiO_2 structure	Xenon lamp, 300 W; filter > 420 nm	GP; CO_2 (1 bar)	CH_4, 2.9	–	119
Pt/TiO_2	Xenon lamp, 300 W, unfiltered	GP; CO_2 (1 bar)	CH_4, 66.4 CO, 54.2	~ 0.04	107

[a] Φ of the apparent quantum efficiency (our estimate). [b] GP is the gas-phase reduction with saturated vapour pressure.

3.1.2.5. Modification with carbon materials

It was noted above that the deposition of metal nanoparticles on the TiO_2 surface is among the most well-tested methods for increasing the photocatalytic activity of systems. Nevertheless, it was found that metals can be partially replaced by some carbonaceous materials like carbon nanotubes or nanosheets, which have a number of advantages such as high corrosion stability and availability. Furthermore, the use of carbon structures during the synthesis of photocatalysts makes it possible to obtain photocatalytically active materials with specified specific surface area and electrical conductivity and with various surface properties.[157–159]

3.1.3. Comparison of activities of titanium dioxide-based photocatalysts

A clear illustration of the progress attained in the photocatalytic reduction of CO_2 in the presence of TiO_2-based photocatalysts is given in Table 2, which presents the results of experiments, including the experimental conditions and types of the light source used.

Analysis of published data on the use of titanium dioxide for the photocatalytic carbon dioxide reduction reveals a high diversity of systems based on both neat and modified TiO_2. Nevertheless, some physical properties of TiO_2 hamper the development of high-performance systems for the photocatalytic CO_2 reduction. This stimulates the search for photocatalytically active materials with optimal properties and optimization of their composition and the ability to absorb light. It is beyond doubt that the potential of systems based on titanium dioxide in the field of photocatalytic fixation of CO_2 is far from being exhausted.

It is evident that modification of titanium dioxide can be either beneficial or detrimenal for the photocatalytic system. It is more appropriate to combine various types of modification. Particularly surface modification of titanium dioxide can be considered as a potential method for controlling the selectivity of the photocatalytic CO_2 reduction to various carbon-containing products.

3.2. Photocatalysts based on cadmium sulfides

Cadmium sulfide is a widely used semiconductor photocatalyst for the hydrogen production from water [165, 166] and for photoreduction of CO_2.[167, 168] Owing to relatively small band gap (~2.4 eV), CdS is highly sensitive to visible light.[169] For photocatalytic applications, solid solutions based on cadmium sulfide and a wider-band semiconductor, for example, mixed cadmium and zinc sulfide ($Zn_xCd_{1-x}S$), are considered to be most efficient.[169] It is notable that the band structure of the $Zn_xCd_{1-x}S$ solid solutions can be finely tuned by changing the Zn : Cd molar ratio.

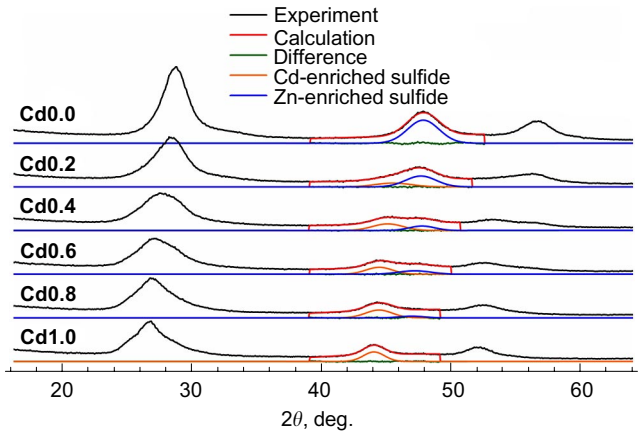


Figure 5. Powder X-ray diffraction patterns of photocatalysts based on zinc and cadmium sulfides.[170] Published with permission from the Royal Society of Chemistry.

Table 3. Phase composition of $Cd_{1-x}Zn_xS-Cd_{1-y}Zn_yS$.[170]

Predetermined atomic fraction of cadmium (%)	Phase composition	a, Å	x	$\langle D\rangle$, nm	Mole fraction of phases (%)
100 (**Cd1.0**)	CdS	5.83	0	4.6	100
80 (**Cd0.8**)	$Cd_{0.91}Zn_{0.09}S$	5.48	0.09	3.0	88
	$Cd_{0.20}Zn_{0.80}S$	5.79	0.80	3.6	12
60 (**Cd0.6**)	$Cd_{0.89}Zn_{0.11}S$	5.46	0.11	3.1	58
	$Cd_{0.16}Zn_{0.84}S$	5.78	0.84	3.7	42
40 (**Cd0.4**)	$Cd_{0.71}Zn_{0.29}S$	5.41	0.96	3.2	53
	$Cd_{0.04}Zn_{0.96}S$	5.70	0.29	3.2	47
20 (**Cd0.2**)	$Cd_{0.59}Zn_{0.41}S$	5.41	0.96	3.2	29
	$Cd_{0.04}Zn_{0.96}S$	5.65	0.31	2.7	71
0 (**Cd0.0**)	ZnS	5.39	1	3.2	100

None. a is cubic unit cell parameter, D is the coherent scattering region.

We studied a series of samples based on both single-phase CdS or ZnS or solid solutions of these sulfides obtained by precipitation from soluble salts of the corresponding metals.[170] According to powder X-ray diffraction data, the prepared samples were $Cd_{1-x}Zn_xS-Cd_{1-y}Zn_yS$ solid solutions (Fig. 5 and Table 3) composed of two phases: $Cd_{0.59}Zn_{0.41}S-Cd_{0.04}Zn_{0.96}S$ (**Cd0.2**), $Cd_{0.71}Zn_{0.29}S-Cd_{0.04}Zn_{0.96}S$ (**Cd0.4**), $Cd_{0.89}Zn_{0.11}S-Cd_{0.16}Zn_{0.84}S$ (**Cd0.6**) and $Cd_{0.91}Zn_{0.09}S-Cd_{0.20}Zn_{0.80}S$ (**Cd0.8**).

The measured band gap widths were 3.6 (345 nm) for ZnS and 2.3 eV (540 nm) for CdS, while for solid solutions **Cd0.8–Cd0.2**, it varied from 2.4 to 2.8 eV, which corresponds to a red absorption edge at 440 to 515 nm. When a light emitting diode with an emission maximum at 450 nm was used as the source of radiation, the rates of carbon dioxide reduction in the presence of ZnS (**Cd0.0**) and **Cd0.2** photocatalysts were close to zero, because the absorption edge of these samples is 350–440 nm.

The specific surface areas of the $Cd_xZn_{1-x}S$ samples were in the range from 96 to 193 $m^2\,g^{-1}$; these are high values for solid solutions of cadmium and zinc sulfides.[169]

The photocatalytic activity of the catalysts based on solid solutions of zinc and cadmium sulfides was studied by carrying out the CO_2 reduction in the presence of saturated water vapour in a static reactor under irradiation at 450 nm. The products identified after the reduction of carbon dioxide and decomposition of water were CO, CH_4 and H_2 (Fig. 6). It is noteworthy that identification of molecular oxygen — the second possible product of water decomposition — was complicated by incomplete tightness of the reactor and getting of traces of air into the reactor during sampling.[170]

In the case of photocatalysts **Cd0.4–Cd1.0**, the dependence of the hydrogen formation rate on the atomic fraction of zinc has a maximum: the highest activity (0.22 $\mu mol\,g^{-1}\,h^{-1}$ for methane and 2.9 $\mu mol\,g^{-1}\,h^{-1}$ for CO) at 95% selectivity of CO_2 reduction was observed for

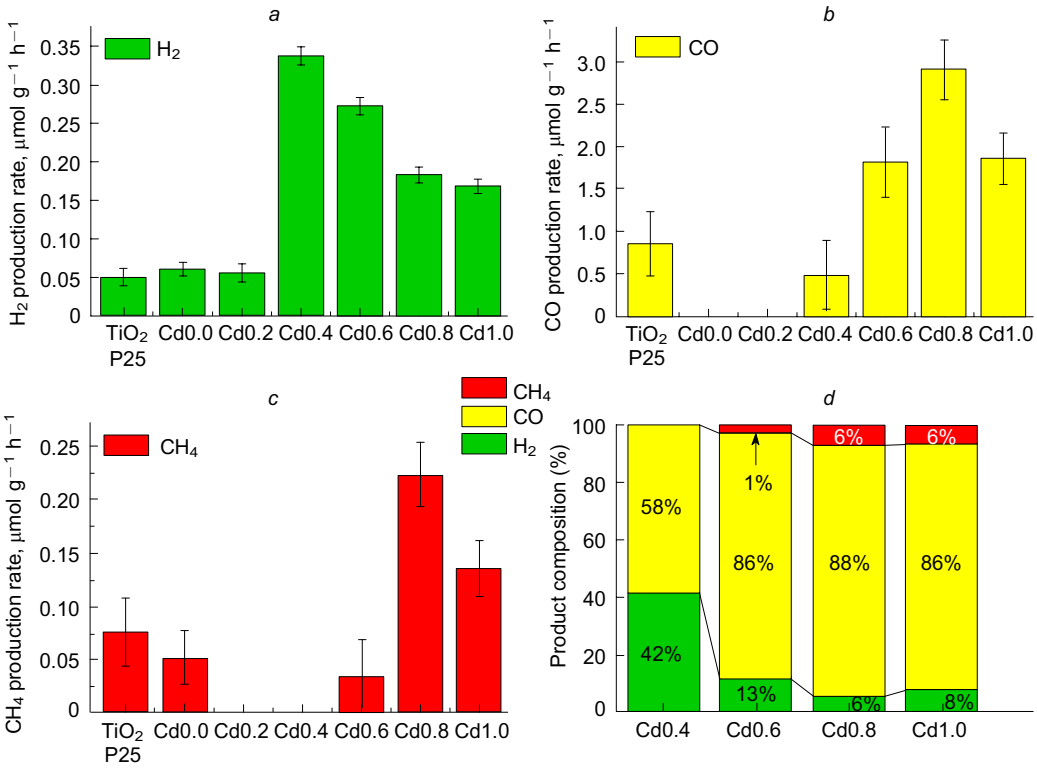


Figure 6. Production rates of H_2 (*a*), CO (*b*) and CH_4 (*c*) and relative distribution of CO_2 reduction products (*d*) formed over photocatalysts based on zinc and cadmium sulfides and TiO_2 Degussa P25 under irradiation with visible light at $\lambda = 450$ nm. Conditions: mixtures of CO_2 and saturated vapour pressure (1 bar, 25 °C).[170] Published with permission from the Royal Society of Chemistry.

Cd0.8. It is known that introduction of zinc into cadmium sulfide induces a blue shift of the absorption edge of the semiconductor; as a result, light absorption at $\lambda = 450$ nm decreases. Hence, the rate of the photocatalytic reactions is expected to decrease. However, the efficiency of photocatalytic reduction of carbon dioxide and decomposition of water depends not only on the band gap width, but also on the position of the conduction band bottom (E_{CB}). Since the addition of zinc to cadmium sulfide increases E_{CB}, the reducing ability of photogenerated electrons increases; hence, the photocatalytic reactions associated with reduction are accelerated.[171] By adjusting the balance between the band gap width and position of the conduction band of mixed sulfide semiconductors, one can prepare active photocatalytic systems based on $Cd_{1-x}Zn_xS$. It is noteworthy that the rates of photocatalytic CO_2 reduction in the presence of synthesized samples were markedly higher than the known values for photocatalysts formed by single zinc and cadmium sulfides.[172]

Subsequently, the deposition of co-catalysts such as NiS [173] and noble metals (Ag and Pt) on the surface of the most active **Cd0.8** sample was studied.[174]

Metallic co-catalysts (Ag and Pt) were deposited by reduction of metal precursors with sodium borohydride (below these samples are designated by 1% Ag/CZS $NaBH_4$ and 1% Pt/CZS $NaBH_4$).[174] The metal deposition on sulfide photocatalysts by this method gave a co-catalyst in the Pt^0/Pt^{2+} oxidation state for platinum and in the Ag^0 and Ag^+ oxidation states in the case of silver. The photocatalytic activity of the synthesized samples was tested in the gas-phase reduction of carbon dioxide in the presence of water vapour under visible light irradiation at $\lambda = 450$ nm (Table 4). It was shown that deposition of platinum or silver on the zinc and cadmium sulfide solid solution leads to a more than twofold decrease in the photocatalyst activity.

Table 4. Production rate of H_2, CO and CH_4 in the presence of photocatalysts based on zinc and cadmium sulfides under visible light irradiation at $\lambda = 450$ nm (according to Lyulyukin *et al.*[174]).

Photocatalyst	Co-catalyst	S_{sp}, $m^2\,g^{-1}$ (see [a])	W, $\mu mol\,g^{-1}\,h^{-1}$			W_{tot} (CO_2), $\mu mol\,g^{-1}\,h^{-1}$ (see [b])
			CH_4	CO	H_2	
Cd0.8	–	119	0.22	2.9	0.18	7.6
1% Pt/**Cd0.8** $NaBH_4$	Pt^0, Pt^{2+}	119	0.24	0.53	0.03	2.9
1% Ag/**Cd0.8** $NaBH_4$	Ag^0, Ag^+	119	0.22	0.90	0.17	3.6

Note. Reaction conditions: a mixture of CO_2 with saturated water vapour (1 bar, 25°C). [a] S_{sp} is the specific surface area of the catalyst surface.[b] The total rate of CO_2 reduction was calculated by the formula:

$$W_{tot}(CO_2) = \frac{8n(CH_4) + 2n(CO)}{tm}$$, where $n(CH_4)$ and $n(CO)$ are the amounts of the formed methane and carbon monoxide, t is the reaction time, m is the photocatalyst mass.

Presumably, the deposited metal particles may act in this case as electron–hole recombination centres, thus decreasing the CO_2 reduction rate. One more issue is that the deposition of indicated metals on the surface of the zinc and cadmium sulfide solid solution leads to higher proportion of methane in the CO_2 reduction products; however, the rate of methane formation remains the same. Apparently, deposited Ag and Pt particles act as transporters of electrons and adsorbed hydrogen atoms and thus catalyze multielectron reduction of CO_2 to CH_4.[174]

Kozlova *et al.*[173] investigated the carbon dioxide reduction in the presence of water vapour and NiS-modified photocatalyst **Cd0.8**. Two series of samples of the ZnS and CdS solid solution with the Cd to Zn atomic ratio of 8 : 2, either bulk- or surface-modified with nickel sulfide, were prepared. In the case of bulk modification, the ternary solid solution of cadmium, nickel and zinc sulfides was obtained by precipitation of metal hydroxides by treatment with sodium hydroxide in the presence of excess sodium sulfide. The $Cd_{0.8}Zn_{0.2}Ni_{x/100}S_{1+x}/100$ samples ($x = 0.05–0.5$) are designated below as **Cd0.8-xb**. In the case of surface modification, nickel sulfide was deposited onto suspended **Cd0.8** from soluble nickel salts on treatment with sodium sulfide. The $x\,NiS–Cd_{0.91}Zn_{0.09}S–Cd_{0.20}Zn_{0.80}S$ samples ($x = 0.1–1.0$) are designated below as **Cd0.8-xs**.

Like in the case of the **Cd0.8** photocatalyst, powder X-ray diffraction analysis[170] revealed the presence of $Cd_{0.91}Zn_{0.09}S$ and $Cd_{0.20}Zn_{0.80}S$ phases (Fig. 7 *a*,*c*). It turned out that deposition of nickel in low concentrations does not affect the powder X-ray diffraction patterns of the samples, but leads to a minor decrease (from 2.42 to 2.37 eV) in the band gap width in the Tauc plots (Fig. 7 *b*,*d*).

The addition of small amounts of nickel sulfide, 0.1 at.% ($0.1\%NiS–Cd_{0.9}Zn_{0.1}S–Cd_{0.2}Zn_{0.8}S$) or 0.05 at.% ($Ni_{0.0005}Cd_{0.9}Zn_{0.1}S_{1.0005}–Cd_{0.2}Zn_{0.8}S$), enhance the activity of the photocatalyst (Fig. 8 and 9). Previously, it was shown[175] that NiS particles deposited on the NiS/$Cd_{1-x}Zn_xS$ photocatalyst can serve as electron transporters and thus increase the activity of solid solutions of zinc and cadmium sulfides in photocatalytic processes.

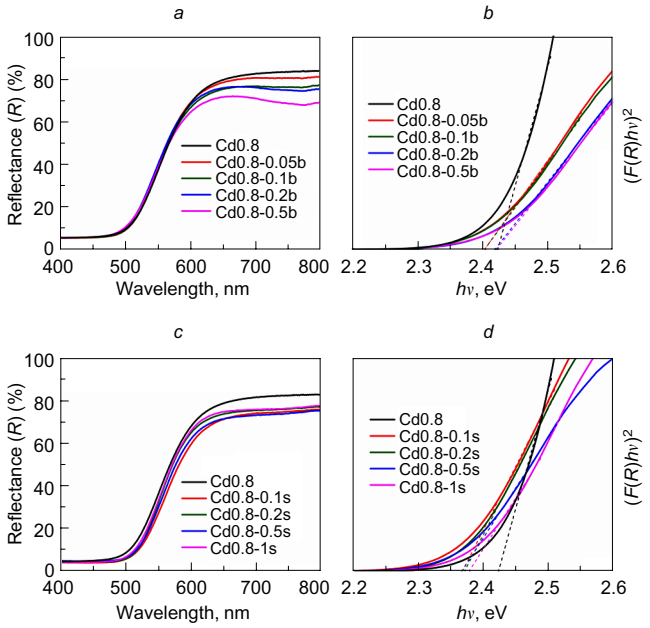


Figure 7. Diffuse reflectance spectra and Tauc plots pf the photocatalysts based on a solid solution of zinc and cadmium sulfides (**Cd0.8**) bulk-modified (**Cd0.8**-xb) (*a*, *b*) and surface-modified (**Cd0.8**-xs) (*c*, *d*) with NiS.[173] Published with permission from Springer.

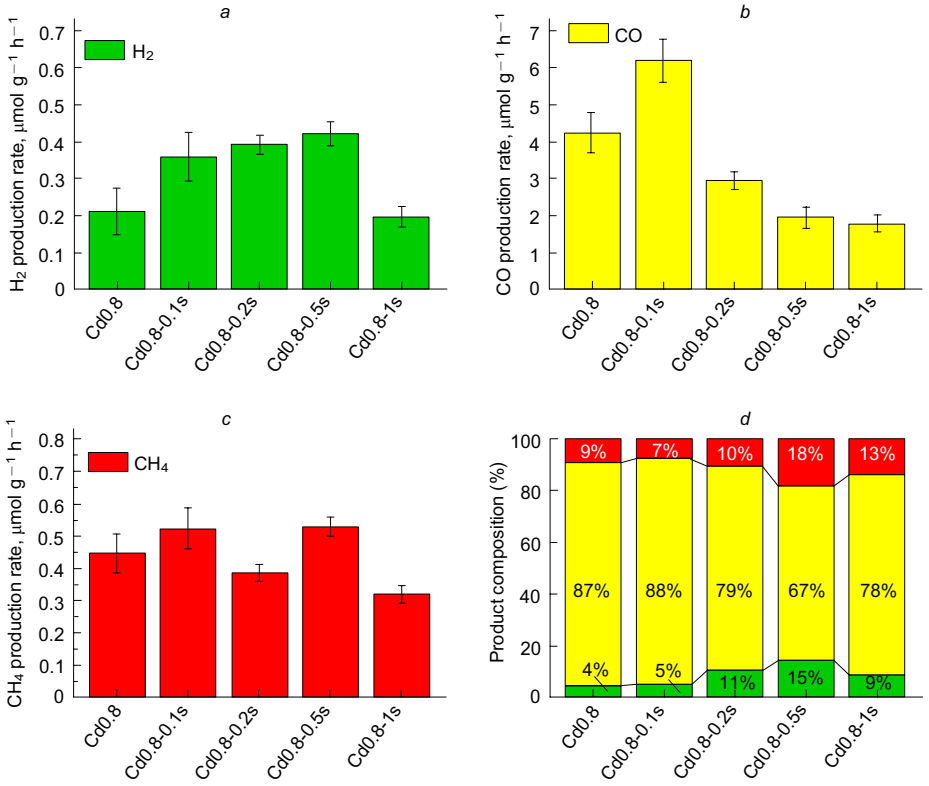


Figure 8. Production rates of H_2 (*a*), CO (*b*) and CH_4 (*c*) and relative distribution of products of gas-phase CO_2 reduction (*d*) in the presence of saturated vapor pressure and a photocatalyst based on a zinc and cadmium sulfide solid solution (**Cd0.8**) surface-modified with NiS under visible light irradiation at $\lambda = 450$ nm.[173] Reaction conditions: CO_2, H_2O (gas.) (1 bar, 25 °C). Published with permission from Springer.

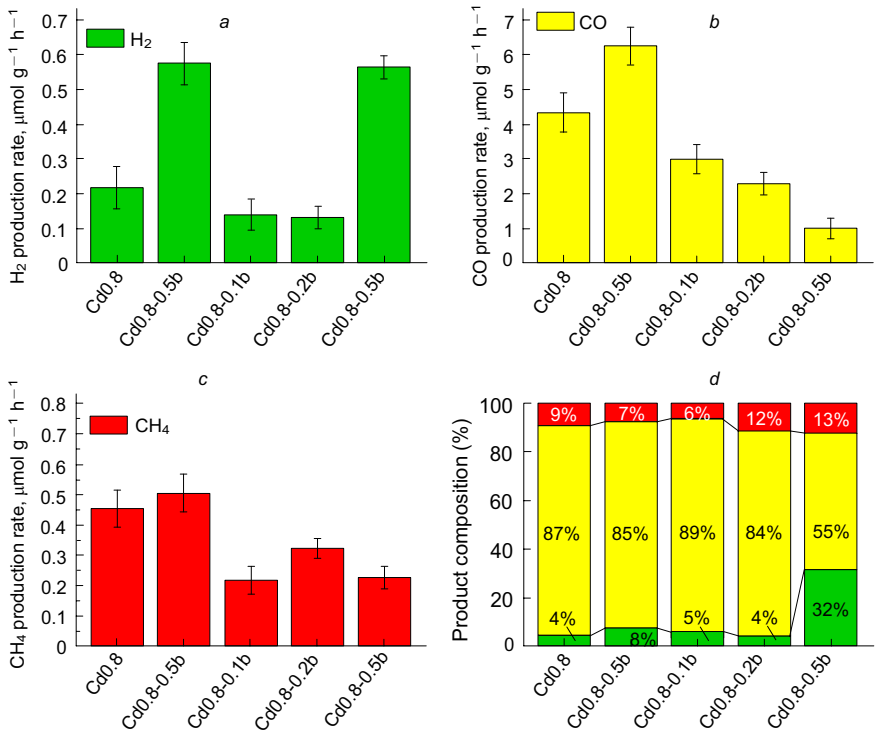


Figure 9. Production rates of H_2 (*a*), CO (*b*) and CH_4 (*c*) and relative distribution of products of gas-phase CO_2 reduction (*d*) in the presence of saturated vapor pressure and a photocatalyst based on a zinc and cadmium sulfide solid solution (**Cd0.8**) bulk-modified with NiS under visible light irradiation at $\lambda = 450$ nm.[173] Reaction conditions: CO_2, H_2O (gas.) (1 bar, 25 °C). Published with permission from Springer.

Table 5. Data on the photocatalytic reduction of carbon dioxide in the presence of photocatalysts based on cadmium sulfide.

Photocatalyst	Light source, electric power, irradiation conditions	Process conditions	Product, rate, μmol g^{-1} h^{-1}	Φ (%)	Ref.
CdS	Xenon lamp, 300 W; filter $\lambda > 400$ nm	Suspension of 1.0 M $NaHCO_3$ (pH 8.0); CO_2 (1 bar)	CH_3OH, 3.8 CH_3CHO, 3.4	~0.04	169
$Cd_{0.2}Zn_{0.8}S$	Xenon lamp, 300 W; filter $\lambda > 400$ nm	Suspension of 1.0 M $NaHCO_3$ (pH 8.0); CO_2 (1 bar)	CH_3OH, 2.5 CH_3CHO, 16.5 CH_3CH_2OH, 6.0	~0.15	169
Nitrogen-doped graphene – CdS	Xenon lamp, 350 W; filter $\lambda > 420$ nm	GP; CO_2 (1 bar)	CO, 2.59 CH_4, 0.33	–0.003	177
CdS – $CdWO_4$	Xenon lamp, 300 W; unfiltered	GP; CO_2 (1 bar)	CO, 1.39 CH_4, 1.50	~0.001	176
$CuGaS_2$ – CdS	Xenon lamp, 300 W; filter $\lambda > 420$ nm	Suspension of 0.1 M K_2SO_3 + 0.5 M $KHCO_3$; CO_2 (1 bar)	CO, 0.75	–	178
CdS – NH_2-UiO-66	Xenon lamp, 300 W; filter $\lambda > 400$ nm	GP; CO_2 (1 bar); addition of triethanolamine	CO, 17.6	–	179
CdS	Xenon lamp, 500 W; filter $\lambda > 400$ nm	Suspension of 0.1 M NaOH + 0.1 M Na_2SO_3; CO_2 (1 bar)	CH_3OH, 40	~0.4	168
Bi_2S_3	Xenon lamp, 500 W; filter $\lambda > 400$ nm	Suspension of 0.1 M NaOH + 0.1 M Na_2SO_3; CO_2 (1 bar)	CH_3OH, 64	~0.7	168
Bi_2S_3 – CdS	Xenon lamp, 500 W; filter $\lambda > 400$ nm	Suspension of 0.1 M NaOH + 0.1 M Na_2SO_3; CO_2 (1 bar)	CH_3OH, 123	~1.1	168
CdS – $BiVO_4$	Xenon lamp, 300 W; filter $\lambda > 400$ nm	GP; CO_2 (3 bar)	CH_4, 1.75 CO, 0.39	–	180
$Cd_{0.9}Zn_{0.1}S$ – $Cd_{0.2}Zn_{0.8}S$	Light-emitting diode source, 30 W; $\lambda = 450$ nm	GP; CO_2 (1 bar)	CO, 0.35 CH_4, 4.2	~0.004	173
0.1%NiS – $Cd_{0.9}Zn_{0.1}S$ – $Cd_{0.2}Zn_{0.8}S$	Light-emitting diode source, 30 W; $\lambda = 450$ nm	GP; CO_2 (1 bar)	CO, 0.53 CH_4, 6.2	~0.006	173
$Ni_{0.0005}Cd_{0.9}Zn_{0.1}S_{1.0005}$ – $Cd_{0.2}Zn_{0.8}S$	Light-emitting diode source, 30 W; $\lambda = 450$ nm	GP; CO_2 (1 bar)	CO, 0.49 CH_4, 6.1	~0.0055	173

In the case of bulk modification of $Cd_{1-x}Zn_xS$ to give ternary solid solutions $Ni_yCd_{1-x}Zn_xS_{1+y}$ solid solutions, the increase in the activity is due to the formation of new energy levels, which can trap photogenerated electrons, thus suppressing the electron–hole recombination.[175]

It is noteworthy that the rates of formation of carbon monoxide (6 μmol g^{-1} h^{-1}) and methane (0.5 μmol g^{-1} h^{-1}) catalyzed by $0.1\%NiS-Cd_{0.9}Zn_{0.1}S-Cd_{0.2}Zn_{0.8}S$ and $Ni_{0.0005}Cd_{0.9}Zn_{0.1}S_{1.0005}-Cd_{0.2}Zn_{0.8}S$ under visible light irradiation proved to be higher than these characteristics for other systems of this type.[176, 177]

The known activities of various photocatalysts based on cadmium sulfide in the CO_2 reduction are summarized in Table 5. It can be seen from the Table that the gas-phase reduction of carbon dioxide gives mainly methane and carbon monoxide and that the measured activities are approximately several micromoles of products per hour per gram of the photocatalyst. More complex products, alcohols and aldehydes, are detected for reactions carried out using photocatalysts suspened in alkaline solutions. However, under these conditions, too, the absolute rates of formation of carbon-containing products are moderate.

3.3. Photocatalysts based on graphitic carbon nitride g-C_3N_4

Polymeric graphitic carbon nitride (g-C_3N_4) is currently considered as an efficient new-generation photocatalyst, which is more active in various photoinduced reactions than traditional photocatalysts such as TiO_2, ZnO and WO_3.[37]

Graphite-like carbon nitride can be synthesized using readily available nitrogen compounds such as melamine and carbamide.[181] It is deemed that g-C_3N_4 has a two-dimensional graphite structure composed of π-conjugated graphite planes, in which the carbon and nitrogen atoms are sp^2-hybridized. Graphite-like carbon nitride is a semiconductor with a band gap of 2.7 eV, highly stable in both acidic and alkaline media. It is noteworthy that, unlike photocatalysts based on transition metal sulfides, g-C_3N_4 is environmentally safe.[182] Due to the above reasons, graphitic carbon nitride is currently one of the most demanded non-oxide and non-sulfide photocatalysts.

Photocatalysts based on g-C_3N_4 are being actively tested in the carbon dioxide reduction processes. The photocatalytic activity of g-C_3N_4 can be increased by using common strategies: fabrication of heterostructures based on g-C_3N_4, varation of the porous structure of the photocatalyst by hydrothermal or template methods and deposition of active co-catalysts on the g-C_3N_4 surface.

The results of recent studies of the photocatalytic reduction of CO_2 in the presence of g-C_3N_4-based photocatalysts are summarized in Table 6.

Like in the case of cadmium sulfide-based photocatalysts, in this case, too, the composition of the reaction products depends on whether the process is conducted in the gas phase or in a photocatalyst suspension. Reasonable

Table 6. Data on the photocatalytic reduction of CO_2 in the presence of photocatalysts based on graphite-like carbon nitride g-C_3N_4.

Photocatalyst	Light source, electric power, irradiation conditions	Process conditions	Product, rate, μmol g^{-1} h^{-1}	Φ (%)	Ref.
Bi_2Se_3–g-C_3N_4	Xenon lamp, 300 W; unfiltered	GP; CO_2 (1 bar)	CO, 8.2	~0.01	183
Cu_2ZnSnS_4–Pt–g-C_3N_4	Xenon lamp, 400 W; filter $\lambda > 420$ nm	GP; CO_2 (1 bar)	CO, 17.3 CH_4, 7.9	~0.03	184
g-C_3N_4–CuO@MIL-125(Ti)	Xenon lamp, 300 W; unfiltered	GP; CO_2 (10 bar)	CO, 60 CH_3OH, 332 CH_3COH, 177 C_2H_5OH, 502	–	185
NiS_2–g-C_3N_4	Xenon lamp, 300 W; unfiltered	Aqueous suspension of photocatalyst; CO_2 (1 bar)	CO, 10.7	2	186
g-C_3N_4	Xenon lamp, 300 W; unfiltered	Aqueous suspension of photocatalyst; CO_2 (1 bar)	CO, 2.75	0.5	186
Phosphorus (black) –g-C_3N_4	Xenon lamp, 300 W; unfiltered	Photocatalyst suspension in a mixture of 33% H_2O + 50% acetonitrile + 17% triethanolamine; CO_2 (1 bar)	CO, 188	–	187
g-C_3N_4	Xenon lamp, 300 W; unfiltered	Photocatalyst suspension in a mixture of 33% H_2O + 50% acetonitrile + 17% triethanolamine; CO_2 (1 bar)	CO, 95.5	–	187
Li–g-C_3N_4	Xenon lamp, 300 W; unfiltered	GP; CO_2 (1 bar)	CO, 1.2	–	188
Na–g-C_3N_4	Xenon lamp, 300 W; unfiltered	GP; CO_2 (1 bar)	CO, 1.5	–	188
K–g-C_3N_4	Xenon lamp, 300 W; unfiltered	GP; CO_2 (1 bar)	CO, 2.0	–	188

Table 6 (continued).

Photocatalyst	Light source, electric power, irradiation conditions	Process conditions	Product, rate, $\mu mol\ g^{-1}\ h^{-1}$	Φ (%)	Ref.
$Rb-g\text{-}C_3N_4$	Xenon lamp, 300 W; unfiltered	GP; CO_2 (1 bar)	CO, 2.4	–	188
$Ti_3C_2-g\text{-}C_3N_4$	Xenon lamp, 300 W; filter $\lambda > 420$ nm	GP; CO_2 (1 bar)	CO, 5.19 CH_4, 0.04	~0.001	189
$g\text{-}C_3N_4$	Xenon lamp, 300 W; filter $\lambda > 420$ nm	GP; CO_2 (1 bar)	CO, 0.62 CH_4, 0.02	~0.0002	189
$Pt-In_2O_3-g\text{-}C_3N_4$	Four light-emitting diodes, 3 W each, $\lambda = 420$ nm	Photocatalyst suspension in a 10% aqueous solution of triethanolamine; CO_2 (1 bar)	HCOOH, 63.1 CH_4, 7.9	~0.13	190
$2\%\ Pt-g\text{-}C_3N_4$	Four light-emitting diodes, 3 W each, $\lambda = 420$ nm	Photocatalyst suspension in a 10% aqueous solution of triethanolamine; CO_2 (1 bar)	HCOOH, 20.1 CH_4, 3.5	~0.05	190
$g\text{-}C_3N_4$	Four light-emitting diodes, 3 W each, $\lambda = 420$ nm	Photocatalyst suspension in a 10% aqueous solution of triethanolamine; CO_2 (1 bar)	HCOOH, 15.6 CH_4, 2.6	~0.035	190
$g\text{-}C_3N_4$ with a defective nitrogen structure	Xenon lamp, 300 W; unfiltered	Aqueous suspension of the photocatalyst; CO_2 (1 bar)	CO, 3.9 CH_4, 7.4	~0.02	191
$Cu-g\text{-}C_3N_4$	Xenon lamp, 300 W; filter $\lambda > 350$ nm	GP; CO_2 (0.7 bar)	CO, 10.2	~0.01	192
$g\text{-}C_3N_4$	Xenon lamp, 300 W; filter $\lambda > 350$ nm	GP; CO_2 (0.7 bar)	CO, 3.9	~0.004	192
$Zn_{0.2}Cd_{0.8}S-g\text{-}C_3N_4$	Xenon lamp, 300 W; filter $\lambda > 420$ nm	Aqueous suspension of the photocatalyst; CO_2 (6 bar)	CH_3OH, 11.5	~0.005	193
$g\text{-}C_3N_4$	Xenon lamp, 300 W; filter $\lambda > 420$ nm	Aqueous suspension of the photocatalyst; CO_2 (6 bar)	CH_3OH, 4.2	~0.002	193
$Zn_{0.2}Cd_{0.8}S$	Xenon lamp, 300 W; filter $\lambda > 420$ nm	Aqueous suspension of the photocatalyst; CO_2 (6 bar)	CH_3OH, 4.4	~0.002	193
$Bi-g\text{-}C_3N_4$	Xenon lamp, 300 W; filter $\lambda > 420$ nm	GP; CO_2 (1 bar)	CO, 1.6 CH_4, 0.1	~0.001	194
$g\text{-}C_3N_4$	Xenon lamp, 300 W; filter $\lambda > 420$ nm	GP; CO_2 (1 bar)	CO, 0.5 CH_4, ~0	~0.0003	194

yields of the products of CO_2 reduction are observed only when high-pressure carbon dioxide is used [185] or when triethanolamine is added to the system as an additional, so-called sacrificial, reducing agent.[187, 190] The quantum efficiencies of systems based on the three most popular photocatalysts (TiO_2, CdS and $g\text{-}C_3N_4$) upon visible light irradiation are approximately equal.

3.4. Conclusions about the current state of studies on the photocatalytic reduction of CO_2

The applicability of various semiconductor photocatalysts for the photocatalytic reduction of carbon dioxide has been studied. In recent years, apart from the sulfide and oxide photocatalysts and materials based on carbon nitride polymers described above, considerable attention of researchers has been devoted to materials based on metal-organic frameworks (MOFs) [195 – 199] and original systems based on titanium carbide, Ti_3C_2 (Ref. 200) or copper(I) oxide.[201] Most of the above results cannot be compared, as they were obtained using markedly different light intensities and spectral compositions, different amounts of absorbed light and different catalyst loadings and either using or not using an additional sacrificial electron donor. The recorded rates of formation of carbon-containing products reach hundreds of micromoles of a product per gram of the photocatalyst for both UV and visible light irradiation. The quantum efficiency values commonly accepted for heterogeneous photocatalytic reactions are presented only in some publications,[45, 115, 202] and reliably measured apparent quantum efficiencies of CO_2 reduction to CH_4 and CO do not exceed 1% under visible light irradiation.[45, 202]

Currently, the major part of studies are aimed at increasing the overall efficiency of the photocatalytic reduction of CO_2. Detailed mechanism of this reaction has not yet been clarified and needs to be further investigated. One can hope that determination of the real reaction pathway and intermediate steps for the photocatalytic CO_2 reduction would allow for more efficient advancement towards the synthesis of useful products from carbon dioxide.

Meanwhile, the accumulated data on the direct photocatalytic reduction of CO_2 over semiconductor photocatalysts demonstrate the need for more serious attitude to the experience of Nature, which was able to develop a much more efficient processes of photosynthesis and CO_2 reduction to organic compounds, for example, *via* the known Calvin cycle.[203] Unfortunately, there is no information on attempt to artificially follow the Nature's way.

4. Reduction of molecular nitrogen in the presence of semiconductor photocatalysts

Molecular nitrogen is the predominant component of air and also the starting block for the synthesis of amino acids, nucleotides and other important biological components for virtually any living organisms. Many nitrogen-binding reactions are thermodynamically admissible under certain conditions. For example, the synthesis of ammonia using hydrogen is a highly exothermic reaction

$$N_2 + H_2 \rightarrow 2\,NH_3,\ \Delta H^0_{r,298} = -92.2\ kJ\,mol^{-1} \quad (1)$$

Nevertheless, this reaction does not proceed spontaneously under ambient conditions, as it requires high pressure. Partially reduced nitrogen compounds, diazine (N_2H_2) and hydrazine (N_2H_4), are not formed spontaneously either. The only abiogenic process of nitrogen fixation under natural conditions is its oxidation with air oxygen in high-temperature plasma formed upon lightning discharge. Nitrogen fixation processes similar to plasma oxidation but induced by light can also occur in the stratosphere on exposure to hard UV radiation.

The catalytic nitrogen fixation (Ref. 1) is actively used to obtain ammonia, a valuable product and reagent.

The major obstacle on the way to successful dark reactions of nitrogen binding is the necessity of activating the N_2 molecule, like the CO_2 molecule. The cleavage of only the first bond in the nitrogen molecule requires an energy of 410 kJ mol^{-1}, while the energy needed to cleave the triple bond is 941 kJ mol^{-1} (Ref. 204). Nevertheless, the Haber (Haber–Bosch) process for ammonia production from a nitrogen and hydrogen gas mixture in the presence of iron-based catalysts under very drastic conditions (temperature of >500 °C, pressure >150 bar) was developed and implemented back at the end of the 19th century.[205–208] This provided a potent tool for the industrial use of nitrogen conversion products and saved agriculture from the threat of nitrogen starvation. The importance of this achievement was acknowledged by awarding F.Haber the Nobel Prize in Chemistry in 1918 for the synthesis of ammonia from its elements. During the next 100 years, the conditions of synthesis were made much milder. For example, transition from iron to ruthenium catalysts made it possible to lower the temperature of synthesis down to 450 °C and to reduce the pressure to virtually 60–80 bar. However, due to wide popularity of this process and concomitant considerable energy expenditures, 1.6% of global atmospheric emission of CO_2 is attributed particularly to implementation of the classical process of ammonia synthesis.[205]

Sunlight is an inexhaustible source of energy; therefore, light-initiated processes are promising virtually in all areas of human development. The use of light for nitrogen binding attracted considerable attention after demonstration of the possibility of photocatalytic nitrogen fixation in the presence of titanium dioxide in 1977.[209] The overall reaction of nitrogen reduction to ammonia in the presence of water *via* combination of water splitting and nitrogen reduction using light energy is described by a reaction equation with the transfer of six electrons

$$N_2 + 3\,H_2O \xrightarrow{h\nu} 2\,NH_3 + 1.5\,O_2 \quad (2)$$

The synthesis of ammonia is the most studied application area of the photofixation of nitrogen; therefore, the primary attention in this part of the review is devoted to achievements in this area.

4.1. Mechanism of nitrogen reduction

Generally, the photocatalytic reduction of N_2 involving a semiconductor photocatalyst can be depicted as a sequence of several steps, like the reduction of CO_2. The first step is the spatial separation of a photogenerated electron and a hole, with the electron entering the conduction band of the semiconductor. Then the photogenerated charge carriers can migrate to the surface (or recombine with heat evolution) where they can be oxidized (*e.g.*, H_2O to O_2) or reduced (*e.g.*, H_2O to H_2 or N_2 to NH_3, in a series of multistep reactions involving protons from water). Electrode reactions corresponding to process (2) are presented in Table 7, which also gives the corresponding electrode potentials.[210–212, 127]

Table 7. Standard electrode potentials E^0 of the possible elementary redox reactions of the photofixation of nitrogen in aqueous solutions at pH 7 (According to Van Der Ham *et al.*[212]).

Reaction	E^0, V *vs.* NHE
$H_2O \rightarrow 0.5\,O_2 + 2\,H^+ + 2\,e^-$	0.81
$2\,H^+ + 2\,e^- \rightarrow H_2$	−0.42
$N_2 + e^- \rightarrow N_2^-$	−4.16
$N_2 + H^+ + e^- \rightarrow N_2H$	−3.2
$N_2 + 2\,H^+ + 2\,e^- \rightarrow N_2H_2$	−1.10
$N_2 + 4\,H^+ + 4\,e^- \rightarrow N_2H_4$	−0.36
$N_2 + 5\,H^+ + 4\,e^- \rightarrow N_2H_5^+$	−0.23
$N_2 + 6\,H^+ + 6\,e^- \rightarrow 2\,NH_3$	0.55
$N_2 + 8\,H^+ + 6\,e^- \rightarrow 2\,NH_4^+$	0.27

The possibility of redox reactions is usually assessed by analyzing the energt levels of the adsorbate and the semiconductor.[213–217] The bottom of the conduction band of the semiconductor should located at a more negative energy level than the potential of the electrode reduction of molecular nitrogen, while the valence band should be at a more positive energy level than the oxygen oxidation and transformation potential. Usually, comparisons are made for the corresponding standard electrode potentials, which is actually not quite correct, because the possibility of spontaneous reaction depends on the relationship between the real, but not standard, redox potentials, which strongly depend on the concentrations of the reactants.[218, 219]

Theoretical calculations were undertaken to determine the possible mechanisms of N_2 reduction in the presence of various photocatalysts.[220, 221] Currently, two mechanisms for N_2 conversion to NH_3 are generally accepted: distal and alternating ones.[222] The distal mechanism implies successive addition of a proton (H^+/e^- pair) to one of the atoms of N_2 molecule to give a terminal nitride intermediate

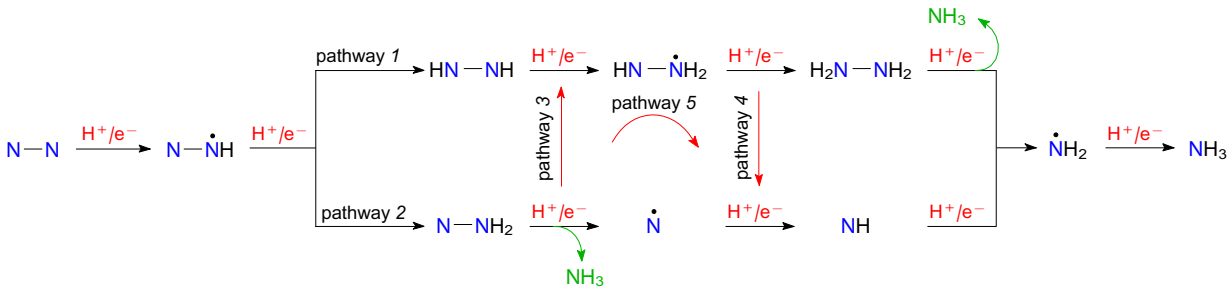


Figure 10. Hypothetical pathways of NH_3 formation from N_2 on the photocatalyst surface.[220] Published with permission from the Royal Society of Chemistry.

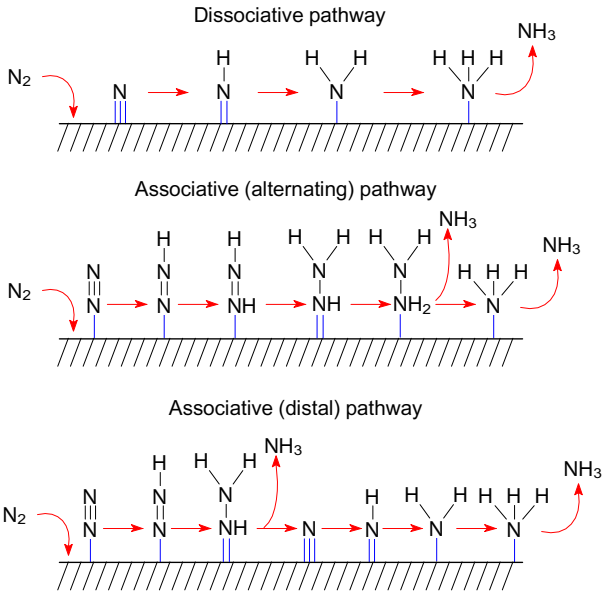


Figure 11. Dissociative and associative pathways to NH_3 from N_2.[223] Published with permission from Elsevier.

capable of liberating the first NH_3 molecule and leaving one nitrogen atom on the photocatalyst surface; finally this atom is converted to one more NH_3 molecule. Conversely, the alternating mechanism implies that the H^+/e^- pairs appear alternately on the two nitrogen atoms of the initial N_2 molecule (Fig. 10).

From the standpoint of traditional catalysis, the possibility of chemisorption of nitrogen molecule on the semiconductor surface opens up two options for the development of the process: dissociative and associative ones. However, owing to the high bond strength in the nitrogen molecule, a dissociative mechanism under ambient conditions cannot be considered as a real option for electrochemical and photocatalytic nitrogen binding systems of ammonia synthesis (Fig. 11).[223]

4.2. Photocatalytic materials for nitrogen reduction

Most of the conventional unmodified semiconductors do not comply with the energy requirements for the photogeneration of charge carriers with reducing potentials appropriate for the reduction of nitrogen. Therefore, a lot of effort was made to choose the nature of semiconductors and to modify them by doping, insertion of vacancies, plasmon induction, lattice adaptation and fabrication of heterostructures in order to improve the photocatalytic characteristics. Classification of known photocatalysts of nitrogen reduction in terms of their elemental composition is presented below.

4.2.1. Metal oxide systems

The advances in the TiO_2-catalyzed photolysis of water[24] initiated the interest in the possibility of photofixation of nitrogen under similar conditions. In 1988, it was found[224] that unmodified TiO_2 shows a photocatalytic activity towards N_2 reduction in the gas phase if it has been initially annealed in air, because thermal pretreatment gives rise to surface defects such as Ti^{3+} ions, producing defective or impurity states in the semiconductor band gap. The arising surface vacancies were systematically studied, regarding their participation in the photocatalytic conversion of N_2 to NH_3, by Hirakawa *et al.*[225] Among the studied TiO_2-based photocatalysts, the highest activity towards nitrogen fixation was found for the rutile phase. Later, it was shown that deposition of Ru, Pt or Pd nanoparticles on TiO_2 does not increase the yield of NH_3, because metal particles cover the Ti^{3+} defects and thus reduce the number of potentially active sites. The surface Ti^{3+} ion can act as the active site for N_2 fixation by donating an electron and facilitating dissociation of the triple bond in the nitrogen molecule. After the reaction, Ti^{3+} can be regenerated under UV irradiation in the presence of an appropriate electron donor.

Considerable progress in N_2 photofixation was attained using photocatalysts based on oxides of other metals such as iron,[226–228] tungsten,[229] gallium[230] and bismuth.[231]

Janet *et al.*[232] studied the photofixation of N_2 in the presence of Pt—ZnO; the authors used commercial zinc oxide and also zinc oxide synthesized by precipitation from zinc nitrate with a greater specific surface area. The rate of NH_3 formation was three times lower in the former case than in the latter case. This may be caused by the fact that, although the platinum contents were equal (1 mass %), the surface of the commercial ZnO sample was largely blocked by platinum particles, since the specific surface area of this photocatalyst is only 3 $m^2\ g^{-1}$, which is 6 times lower than the specific surface area of the synthesized ZnO. Generally, it can be concluded that doping of catalytic systems for N_2 photofixation with transition metals promotes higher yield of ammonia.

In the search for the ways for increasing the photocatalytic properties *via* complication of catalytic systems, catalysts based on various metal titanates and other double oxides were investigated. The results of combining titanium and iron by using titanates such as Fe_2TiO_5 were contradictory: according to some data, no photocatalytic activity

was inherent in these systems,[233–235] while other results indicate the opposite.[236] Subsequently, this contradiction was explained by the considerable influence of the method used to prepare the photocatalysts on their characteristics.[237] Currently, systems based on titanium dioxide and various metal titanates predominate among the oxide systems used for N_2 photofixation.[238, 239]

4.2.2. Metal sulfide systems

Small band gaps and, as a consequence, the ability to absorb visible light stimulated the studies of various metal sulfide systems for the photofixation of N_2.

In the 1980s, an ammonia production rate of $\sim$2.2 mol g^{-1} h^{-1} was attained using systems with CdS as the photocatalyst;[240, 241] during the further development of sulfide systems, the production rate of the final products and the quantum efficiency of nitrogen photofixation were substantially increased.[242]

The publication of studies in which N_2 photofixation was attributed to the presence of oxygen vacancies on the catalyst surface as, for example, in BiOBr,[243] was followed by successful insertion of sulfur vacancies into semiconductor sulfide structures. This led to partial chemisorption of nitrogen molecules on the photocatalysts, which finally provided a sort of preactivation of the chemical bond of N_2 and increased the nitrogen reduction rate.[244] In addition, a linear correlation was established between the NH_3 production rate and concentration of the sulfur vacancies (Fig. 12).

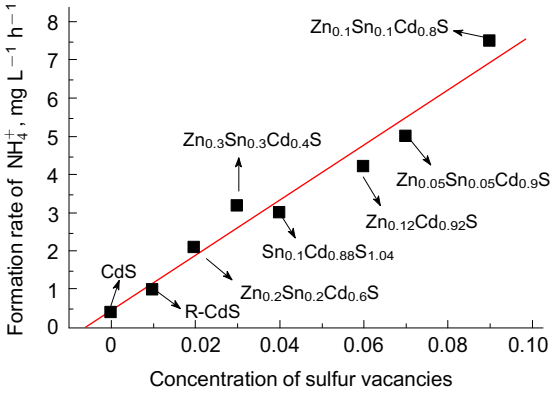


Figure 12. Rate of the photocatalytic fixation of N_2 to give ammonia *vs.* concentration of sulfur vacancies on the catalyst surface.[244] R-CdS is a CdS sample treated with a 1 : 9 H_2–Ar gas mixture (500 °C, 2 h). Published with permission from the Royal Society of Chemistry.

Complex three-component sulfide photocatalysts, $Mo_{0.1}Ni_{0.1}Cd_{0.8}S$, have been studied;[245] this study was continued by the design of g-C_3N_4/ZnMoCdS type heterostructures,[246, 247] in which the heterojunction between g-C_3N_4 and ZnMoCdS was of key importance for the efficient charge separation. The photogenerated electrons migrated from g-C_3N_4 to metal sulfide, whereas the holes moved in the opposite direction. This gaves rise to a permanent internal electric field directed from the sulfide to g-C_3N_4, which decreased the rate of recombination of electrons and holes and finally considerably increased the rate of photocatalytic reduction of N_2 to NH_3.

Unique electrical,[248] optical[249] and optoelectronic properties are inherent in MoS_2,[250] which is a narrow-band gap semiconductor with a 1.2 eV indirect band gap (in the limiting case of multilayer MoS_2, it is displaced by a 1.9 eV direct band gap).[251] This feature was used for the photocatalytic reduction of N_2 to NH_3 in the presence of ultrathin layered MoS_2.[210] A study of the photocatalytic characteristics of MoS_2 samples prepared under various conditions under irradiation at $\lambda > 420$ nm showed that a larger amount of NH_3 is regularly generated on the ultrathin sample. Presumably, excitons formed in a MoS_2 monolayer can trap additional electrons, thus forming charged excitons with two bound electrons, which facilitates multielectron N_2 reduction.[252] In particular, the simultaneous transfer of six electrons on these photocatalysts may account for accelerated reduction of N_2 to NH_3. In this respect, it is pertinent to note that exactly molybdenum sulfide clusters are prosthetic groups of natural nitrogen-fixation enzymes such as nitrogenases.[253]

4.2.3. Bismuth oxyhalides

Bismuth oxyhalides BiOX (X = Cl, Br and I) are used, for example, for photocatalytic degradation of organic pollutants in aqueous solutions under the action of solar light.[254] They are V–VI–VII ternary oxide semiconductors with a specal layered structure, while the formed internal electric field favours efficient separation and transfer of photogenerated charge carriers.[255, 256] In recent years, Bi_5O_7Br type bismuth oxyhalides have been studied as photocatalysts for N_2 fixation under the action of solar light.[144, 243, 257, 258]

The photocatalytic reduction of N_2 under visible light irradiation was carried out using BiOBr samples with oxygen vacancies;[243] the recorded nitrogen fixation rate was 104 μmol g^{-1} h^{-1}. According to the results of theoretical modelling, the presence of oxygen vacancies in BiOB induces elongation of the triple bond in the nitrogen molecule from 1.078 to 1.133 Å, which activates the molecule. In addition, due to the large number of vacancies on the surface, defective states are formed near the bottom of the conduction band of the photocatalyst, which hampers the electron–hole recombination. However, the surface oxygen vacancies are oxidized under the action of light under normal conditions, which leads to gradual decrease in the photocatalyst activity. Li *et al.*[221] studied the photoactivity of oxygen vacancies at different faces of BiOBr. It was shown that nitrogen fixation by oxygen vacancies at the {001} faces corresponds to the distal pathway

$$N_2 \rightarrow N{-}NH_3 \rightarrow N + NH_3 \rightarrow 2\,NH_3$$

whereas fixation at the {010} faces corresponds to the alternating pathway

$$N_2 \rightarrow N_2H_3 \rightarrow N_2H_4$$

Bai *et al.*[259] used nanosheets of bismuth oxyhalide (particularly Bi_5O_7I) in which certain lattice faces, {001} or {101}, predominated. The N_2 photofixation rates were 112 a 47.6 μmol L^{-1} h^{-1}, respectively. The higher rate of NH_3 formation observed at the {001} face was attributed to the more negative potential of the conduction band at the {001} face (−1.45 V *vs.* NHE) than at the {101} face (−0.85 V). Most authors pay considerable attention to

comparison of the properties of different faces of oxyhalides, although it is quite likely that new prospects for the development of efficient photocatalysts for N_2 reduction will be opened by combining the effects of oxygen vacancies and oxyhalide faces. In addition, these studies demonstrated the efficiency of combining the results of experimental studies and theoretical simulation for elucidation of the most probable mechanism of triple bond activation in N_2 molecules and pathways towards NH_3.

4.2.4. Comparative data on the photocatalytic reduction of nitrogen

The published data on the photocatalytic activity of materials tested for N_2 fixation are summarized in Table 8. It can be seen that results of studies may be markedly different and it is difficult to consider them altogether. This is mainly caused by different natures of systems used in the studies. Indeed, the N_2 photofixation rate in gas-phase reactions is expressed in μmol g^{-1} h^{-1}, while for reactions carried out in suspensions, it is measured in μmol L^{-1} h^{-1}. Therefore, for correct comparison of the properties of photocatalytic systems, it is necessary that results are expressed in the same units, *e.g.*, as the apparent quantum efficiency (Φ). This can be used not only to identify the most efficient systems, but also to find out how reaction conditions, such as spectral characteristic and power of the light source, catalyst loading, reaction time and the illuminated surface area, influence the observed efficiency of catalytic systems.

As can be seen from the foregoing, most of published data address nanomaterials based on metal oxides, in particular, TiO_2. However, the photocatalytic activity of TiO_2 is highly restricted by its ability to absorb only UV radiation, which accounts for only a minor part of the solar spectrum that reaches the Earth s surface. In order to expand the photoactive light spectrum, various types of doping and modification of the oxides are employed. Instead of pure nitrogen and UV radiation, the use of air and visible light has been recently considered more and more often.

One more efficient method that may contribute to the spatial separation of photogenerated charge carriers needed for redox reactions to proceed is the use of photoelectrocatalytic systems, which allow for spatially decoupled N_2 reduction and H_2O oxidation reactions on the photocathode and photoanode, respectively. By combining light-induced and electrochemical reactions, it is possible to increase the activity of N_2 reduction catalysts, especially if the photocatalysts are different for the anode and cathode sides. Nevertheless, there are still very few publications reporting successful photoelectrochemical fixation of N_2.

The data collected in Table 8 indicate that over a few decades, the production rates in gas-phase photoreduction of N_2 increased 1000-fold (from μmol g^{-1} h^{-1} to mmol g^{-1} h^{-1}). One can hope that systems providing production rates acceptable for practical application (of the order of mol g^{-1} h^{-1}) will be found in the future. It should be emphasized that despite increasing interest in the photocatalytic fixation of nitrogen in general, most of the studied photocatalytic systems were implemented only on a laboratory scale. Therefore, a key challenge is to attain high production rates of the target products for photocatalysts

Table 8. Data on the photocatalytic reduction of nitrogen to give ammonia in the presence of various photocatalysts.

Photocatalyst	Light source, electric power, irradiation conditions	Medium, conditions	NH_3 production rate, μmol g^{-1} h^{-1}	Φ (%)	Ref.
TiO_2	Mercury lamp, 300 W, unfiltered	N_2, 500 K, GP, H_2O vapour	0.83	–	224
0.4% Co – TiO_2	Mercury lamp, 360 W, unfiltered	N_2, 40 °C, GP, H_2O vapour, 1 atm	6.3	–	209
0.4% Mo – TiO_2	Mercury lamp, 360 W, unfiltered	N_2, 40 °C, GP, H_2O vapour, 1 atm	6.7	–	209
0.4% Cr – TiO_2	Mercury lamp, 360 W, unfiltered	N_2, 40 °C, GP, H_2O vapour, 1 atm	0.37	–	209
2% Mg – TiO_2	Mercury lamp, 400 W, unfiltered	N_2, catalyst (0.2 g) suspension in H_2O (300 mL)	6.9	0.000055	260
0.24% Ru – TiO_2	Xenon lamp, 150 W, unfiltered	N_2, catalyst (0.1 g) suspension in H_2O (20 mL); ethanol as the sacrificial agent	22.7	–	261
Fe_2O_3	Xenon lamp, 150 W, unfiltered	N_2, catalyst (0.03 g) suspension in H_2O (30 mL)	10	0.13	227
$BaTiO_3$	Mercury lamp, 450 W, unfiltered	N_2 (0.9 atm), GP, H_2O vapour	0.87	0.002	262
RuO_2 – NiO – $BaTiO_3$	Mercury lamp, 450 W, unfiltered	N_2 (0.9 atm), GP, H_2O vapour	2.6	0.0073	262
Bi_5O_7Br	Xenon lamp 300 W, filter > 400 nm	N_2, catalyst (0.025 g) suspension in H_2O (100 mL)	1380	2.3	257
$Ni_2P/Cd_{0.5}Zn_{0.5}S$	Xenon lamp 300 W, filter > 400 nm	N_2, catalyst (0.02 g) suspension in H_2O (50 mL)	102	4.3	242
Cs_2O – Os-Au	Solar simulator, 200 mW cm^{-2}, filter ⩾450 nm	N_2/H_2, GP, 15 mL min^{-1} of N_2 and 45 mL min^{-1} of H_2, 1 atm, 60 °C	2685	0.003	263

and simultaneously to design photocatalytic devices that would enable practical use of these photocatalysts.

The results summarized in the review allow one to draw conclusions about the promising trends in the development of photocatalytic systems for nitrogen fixation under the action of solar light. First, a more in-depth understanding of the elementary steps of nitrogen photofixation should be gained; otherwise, targeted improvement of the design of photocatalytic systems is impossible. It is especially important to determine the conditions for the first bond cleavage in the molecular nitrogen and formation of nitrogen – hydrogen bond, which is critically important for identification of the most promising reaction pathways and for the choice of appropriate systems. The results of numerous studies indicate that the presence of oxygen vacancies in semiconductor photocatalysts has a beneficial effect on not only adsorption, but also subsequent activation of N_2 molecule. Also, it can be taken that the rate of reaction in aqueous solutions is limited by low N_2 solubility in water (which is used most often as proton donor). Therefore, the design of photocatalytic systems should also envisage the improvement of nitrogen adsorption on the catalyst. A promising strategy for increasing the performance of photocatalytic systems is to expand the photocatalytic action to the visible region of electromagnetic spectrum, which would increases the efficiency of solar light utilization and the number of elementary charge carriers generated under the action of photons and initiating the sequences of reactions.

An inevitable side reaction of nitrogen reduction in solution in the presence of oxygen is the oxidation of ammonia to NO_3^- and NO_2^-. The undesirable oxidation reactions can be suppressed using photoelectrochemical cells with proton exchange membranes in which water is oxidized at the photoanode, while the photogenerated electrons can be used for the reduction and protonation of ammonia in the cathode side of the system. It is necessary to develop also other, more facile methods for suppression of side reactions that consume the target products of the photocatalytic synthesis.

5. Conclusion

The photocatalytic fixation of carbon dioxide and molecular nitrogen using solar energy is a promising area among the applications of solar energy for the production of useful products with minimum environmental damage. The photocatalytic reduction of carbon dioxide and molecular nitrogen under the action of electromagnetic radiation of various ranges attracts considerable attention of researchers, as evidenced by the large number of publications on this topic over the past decade. The photocatalytic fixation of CO_2 and N_2 is based on the same principles as the much better studied photocatalytic oxidation of organic compounds and production of hydrogen from water and solutions of various substrates. Nevertheless, the activities towards the formation of CO_2 and N_2 reduction products attained to date are still at the level of micromoles per gram of the photocatalyst per hour, which is several orders of magnitude lower than the corresponding values for the photocatalytically induced production of hydrogen.

The photocatalysts tested for the carbon dioxide and nitrogen reduction were mainly typical semiconductors based on titanium dioxide, transition metal sulfides and carbon materials. A considerable obstacle to reaching a high photocatalytic activities in these processes is low adsorption of CO_2 and N_2 molecules on the surface of semiconductor photocatalysts. In addition, apart from the synthesis of active photocatalysts, it is necessary to select the optimal conditions for the process. Recent publications consider the photocatalytic reduction of CO_2 in the presence of not only water, but also sacrificial reducing agents such as hydrogen and triethanolamine. It is obvious that the expediency of using these reducing agents should be specially evaluated, since this appears promising only if this gives more energy-saturated molecules than the products of CO_2 reduction formed with water alone.

In most studies of the photocatalytic reduction of carbon dioxide, the concentration of products of only this reaction is measured. Meanwhile, the products of photocatalytic oxidation (molecular oxygen if water served as the electron donor) are usually not detected. This indicates that CO_2 may be actually reduced by impurities present on the surface of the photocatalyst. Meanwhile, the changes taking place on the photocatalyst surface during the photoprocess are studied quite rarely. A considerable problem for evaluation of the real achievements in the photocatalytic fixation of CO_2 and N_2 is the absence of a generally accepted universal quantity characterizing the activity of photocatalysts, such as the apparent quantum efficiency.[264]

The above data lead to the conclusion that, despite a large body of studies in the photocatalytic conversion of carbon dioxide and molecular nitrogen on semiconductor photocatalysts, there are still a lot of controversial issues in the discussion of the results obtained to date. Nevertheless, these processes certainly require further experimental and theoretical investigation, since their successful implementation would bring closer the possibility of mimicking the most important natural synthetic processes that take place in plants and microorganisms.

The reported study was funded by the Russian Foundation for Basic Research (Project No. 19-13-50251).

6. List of acronyms and designations

CB — conduction band,
CZS — $Cd_{1-x}Zn_xS$,
g-C_3N_4 — graphitic carbon nitride.
GP — has-phase reduction with saturated water vapor,
NHE — normal hydrogen electrode,
VB — valence band,
Φ — apparent quantum efficiency.

References

1. K.C.Christoforidis, P.Fornasiero. *ChemCatChem*, **11**, 368 (2019)
2. N.S.Lewis, D.G.Nocera. *Proc. Natl. Acad. Sci. USA*, **103**, 15729 (2006)
3. A.Makarov, A.Galkina, E.Grushevenko, D.Grushevenko, V.Kulagin, T.Mitrova, S.Sorokin. *Mirovaya Ekonomika i Mezhdunorodnye Otnosheniya*, **1**, 3 (2014)
4. S.Yamaguchi, I.Tokairin, Y.Wakita, Y.Funahashi, K.Jitsukawa, H. Masuda. *Chem. Lett.*, **32**, 406 (2003)
5. J.Wu, R.M.Yadav, M.Liu, P.P.Sharma, C.S.Tiwary, L.Ma, X.Zou, X.Zhou, B.I.Yakobson, J.Lou, P.M.Ajayan. *ACS Nano*, **9**, 5364 (2015)
6. S.Remiro-Buenamañana, H.García. *ChemCatChem*, **11**, 342 (2019)

7. M.Aresta, A.Dibenedetto, A.Angelini. *J. CO_2 Util.*, **3** – **4**, 65 (2013)
8. L.Yuan, M.-Y.Qi, Z.-R.Tang, Y.-J.Xu. *Angew. Chem., Int. Ed.*, **60**, 2 (2021)
9. M.Muringa Kandy, A.Rajeev K, M.Sankaralingam. *Sustain. Energy Fuels*, **5**, 12 (2021)
10. T.Rasheed, S.Shafi, M.T.Anwar, K.Rizwan, T.Ahmad, M.Bilal. *Appl. Catal. A Gen.*, **623**, 118248 (2021)
11. Z.Sun, J.Dong, C.Chen, S.Zhang, Y.Zhu. *J. Chem. Technol. Biotechnol.*, **96**, 1161 (2021)
12. N.Keller, J.Ivanez, J.Highfield, A.M.Ruppert. *Appl. Catal., B*, **296**, 120320 (2021)
13. A.G.Variar, M.S.Ramyashree, V.U.Ail, S.S.Priya, K.Sudhakar, M.Tahir. *J. Ind. Eng. Chem.*, **99**, 19 (2021)
14. J.Low, B.Cheng, J.Yu, M.Jaroniec. *Energy Storage Mater.*, **3**, 24 (2016)
15. S.N.Habisreutinger, L.Schmidt-Mende, J.K.Stolarczyk. *Angew. Chem., Int. Ed.*, **52**, 7372 (2013)
16. A.L.Linsebigler, G.Lu, J.T.Yates. *Chem. Rev.*, **95**, 735 (1995)
17. A.Kubacka, M.Fernández-García, G.Colón. *Chem. Rev.*, **112**, 1555 (2012)
18. J.Li, G.Chen, Y.Zhu, Z.Liang, A.Pei, C.-L.Wu, H.Wang, H.R.Lee, K.Liu, S.Chu, Y.Cui. *Nat. Catal.*, **1**, 592 (2018)
19. D. Raciti, M.Mao, J.H.Park, C.Wang. *Catal. Sci. Technol.*, **8**, 2364 (2018)
20. A.Li, Q.Cao, G.Zhou, B.V.K.J.Schmidt, W.Zhu, X.Yuan, H.Huo, J.Gong, M.Antonietti. *Angew. Chem., Int. Ed.*, **131**, 14691 (2019)
21. K.Ikeue, H.Yamashita, M.Anpo, T.Takewaki. *J. Phys. Chem. B*, **105**, 8350 (2001)
22. X.Chen, N.Li, Z.Kong, W.-J.Ong, X.Zhao. *Mater. Horizons*, **5**, 9 (2018)
23. W.Peng, T.H.Chuong Nguyen, D.L.T.Nguyen, T.Wang, T.Van Thi Tran, T.H.Le, H.K.Le, A.N.Grace, P.Singh, P.Raizadaa, M.T.Nguyen Dinh, C.C.Nguyen, S.Y.Kim, Q.Van Le. *Renew. Sustain. Energy Rev.*, **148**, 111298 (2021)
24. A.Fujishima, K.Honda. *Nature (London)*, **238**, 37 (1972)
25. T.Inoue, A.Fujishima, S.Konishi, K.Honda. *Nature (London)*, **277**, 637 (1979)
26. A.J.Morris, G.J.Meyer, E.Fujita. *Acc. Chem. Res.*, **42**, 1983 (2009)
27. C.C.Yang, Y.-H.Yu, B.Van Der Linden, J.C.S.Wu, G.Mul. *J. Am. Chem. Soc.*, **132**, 8398 (2010)
28. A.Corma, H.Garcia. *J. Catal.*, **308**, 168 (2013)
29. Y.Liu, S.Deng, R.Zhao, J.He, L.Zhao. *Renew. Sustain. Energy Rev.*, **77**, 652 (2017)
30. Y.Kohno, T.Tanaka, T.Funabiki, S.Yoshida. *Phys. Chem. Chem. Phys.*, **2**, 2635 (2000)
31. Y.Kohno, T.Tanaka, T.Funabiki, S.Yoshida. *Phys. Chem. Chem. Phys.*, **2**, 5302 (2000)
32. K.Teramura, S.ichi Okuoka, H.Tsuneoka, T.Shishido, T.Tanaka. *Appl. Catal., B*, **96**, 565 (2010)
33. K.Teramura, H.Tsuneoka, T.Shishido, T.Tanaka. *Chem. Phys. Lett.*, **467**, 191 (2008)
34. S.Navalón, A.Dhakshinamoorthy, M.Álvaro, H.Garcia. *ChemSusChem*, **6**, 562 (2013)
35. P.Johne, H.Kisch. *J. Photochem. Photobiol., A*, **111**, 223 (1997)
36. S.M.Aliwi, K.F.Al-Jubori. *Sol. Energy Mater.*, **18**, 223 (1989)
37. W.K.Darkwah, K.A.Oswald. *Nanoscale Res. Lett.*, **14**, 234 (2019)
38. J.Yang, H.Wang, L.Jiang, H.Yu, Y.Zhao, H.Chen, X.Yuan, J.Liang, H.Li, Z.Wu. *Chem. Eng. J.*, **427**, 130991 (2022)
39. J.Liang, X.Yang, Y.Wang, P.He, H.Fu, Y.Zhao, Q.Zou, X.An. *J. Mater. Chem. A*, **9**, 12898 (2021)
40. L.Ai, R.Shi, J.Yang, K.Zhang, T.Zhang, S.Lu. *Small*, 2007523 (2021)
41. P.Madhusudan, R.Shi, S.Xiang, M.Jin, B.N.Chandrashekar, J.Wang, W.Wang, O.Peng, A.Amini, C.Cheng. *Appl. Catal., B*, **282**, 119600 (2021)
42. A.V.Zhurenok, T.V.Larina, D.V.Markovskaya, S.V.Cherepanova, E.A.Mel'gunova, E.A.Kozlova. *Mendeleev Commun.*, **31**, 157 (2021)
43. M.R.Hoffmann, S.T.Martin, W.Choi, D.W.Bahnemann. *Chem. Rev.*, **95**, 69 (1995)
44. J.Herrmann. *Catal. Today*, **53**, 115 (1999)
45. J.Jiao, Y.Wei, Y.Zhao, Z.Zhao, A.Duan, J.Liu, Y.Pang, J.Li, G.Jiang, Y.Wang. *Appl. Catal., B*, **209**, 228 (2017)
46. Yu.A.Gruzdkov, E.N.Savinov, V.N.Parmon. *Khim. Fiz.*, **7**, 44 (1988)
47. X.Li, J.Yu, J.Low, Y.Fang, J.Xiao, X.Chen. *J. Mater. Chem. A*, **3**, 2485 (2015)
48. A.Cybula, M.Klein, A.Zaleska. *Appl. Catal., B*, **164**, 433 (2015)
49. C.C.Lo, C.H.Hung, C.S.Yuan, J.F.Wu. *Sol. Energy Mater. Sol. Cells*, **91**, 1765 (2007)
50. Y.Ku, W.H.Lee, W.Y.Wang. *J. Mol. Catal., A*, **212**, 191 (2004)
51. L.Chen, M.E.Graham, G.Li, D.R.Gentner, N.M.Dimitrijevic, K.A.Gray. *Thin Solid Films*, **517**, 5641 (2009)
52. B.Ohtani, O.O.Prieto-Mahaney, D.Li, R.Abe. *J. Photochem. Photobiol., A*, **216**, 179 (2010)
53. D.Gumy, S.A.Giraldo, J.Rengifo, C.Pulgarin. *Appl. Catal., B*, **78**, 19 (2008)
54. D.C.Hurum, K.A.Gray, T.Rajh, M.C.Thurnauer. *J. Phys. Chem. B*, **109**, 977 (2005)
55. D.C.Hurum, A.G.Agrios, K.A.Gray, T.Rajh, M.C.Thurnauer. *J. Phys. Chem. B*, **107**, 4545 (2003)
56. K.Komaguchi, H.Nakano, A.Araki, Y.Harima. *Chem. Phys. Lett.*, **428**, 338 (2006)
57. T.Ohno, K.Sarukawa, K.Tokieda, M.Matsumura. *J. Catal.*, **203**, 82 (2001)
58. T.Kawahara, Y.Konishi, H.Tada, N.Tohge, J. Nishii, S.Ito. *Angew. Chem., Int. Ed.*, **41**, 2811 (2002)
59. J. Zhang, Q.Xu, Z.Feng, M.Li, C.Li. *Angew. Chem., Int. Ed.*, **47**, 1766 (2008)
60. B.Sun, P.G.Smirniotis. *Catal. Today*, **88**, 49 (2003)
61. L.Jing, S.Li, S.Song, L.Xue, H.Fu. *Sol. Energy Mater. Sol. Cells*, **92**, 1030 (2008)
62. S.Leytner, J.T.Hupp. *Chem. Phys. Lett.*, **330**, 231 (2000)
63. S.S.Tan, L.Zou, E.Hu. *Catal. Today*, **115**, 269 (2006)
64. M.Gattrell, N.Gupta, A.Co. *J. Electroanal. Chem.*, **594**, 1 (2006)
65. H.He, P.Zapol, L.A.Curtiss. *Energy Environ. Sci.*, **5**, 6196 (2012)
66. M.Subrahmanyam, S.Kaneco, N.Alonso-Vante. *Appl. Catal., B*, **23**, 169 (1999)
67. N.M.Dimitrijevic, B.K.Vijayan, O.G.Poluektov, T.Rajh, K.A.Gray, H.He, P.Zapol. *J. Am. Chem. Soc.*, **133**, 3964 (2011)
68. K.Ikeue, S.Nozaki, M.Ogawa, M.Anpo. *Catal. Today*, **74**, 241 (2002)

69. O.K.Varghese, M.Paulose, T.J.LaTempa, C.A.Grimes. *Nano Lett.*, **9**, 731 (2009)
70. H.Yamashita, Y.Fujii, Y.Ichihashi, S.G.Zhang, K.Ikeue, D.R.Park, K.Koyano, T.Tatsumi, M.Anpo. *Catal. Today*, **45**, 221 (1998)
71. S.S.Tan, L.Zou, E.Hu. *Catal. Today*, **131**, 125 (2008)
72. I.A.Shkrob, T.W.Marin, H.He, P.Zapol. *J. Phys. Chem. C*, **116**, 9450 (2012)
73. I.A.Shkrob, N.M.Dimitrijevic, T.W.Marin, H.He, P.Zapol. *J. Phys. Chem. C*, **116**, 9461 (2012)
74. E.Barton Cole, P.S.Lakkaraju, D.M.Rampulla, A.J.Morris, E.Abelev, A.B.Bocarsly. *J. Am. Chem. Soc.*, **132**, 11539 (2010)
75. E.Korovin, D.Selishchev, D.Kozlov. *Top. Catal.*, **59**, 1292 (2016)
76. A.Meisen, X.Shuai. *Energy Convers. Manag.*, **38**, 37 (1997)
77. M.H.N.Assadi, D.A.H.Hanaor. *Appl. Surf. Sci.*, **387**, 682 (2016)
78. E.M.Samsudin, S.B.Abd Hamid, J.C.Juan, W.J. Basirun, G.Centi. *Appl. Surf. Sci.*, **370**, 380 (2016)
79. E.Shin, S.Jin, J.Kim, S.-J.Chang, B.-H.Jun, K.-W.Park, J.Hong. *Appl. Surf. Sci.*, **379**, 33 (2016)
80. S.Das, W.M.A.Wan Daud. *RSC Adv.*, **4**, 20856 (2014)
81. Q.Zhang, D.Q.Lima, I.Lee, F.Zaera, M.Chi, Y.Yin. *Angew. Chem., Int. Ed.*, **123**, 7226 (2011)
82. C.Han, M.Pelaez, V.Likodimos, A.G.Kontos, P.Falaras, K.O'Shea, D.D.Dionysiou. *Appl. Catal., B*, **107**, 77 (2011)
83. M.Khan, J.Xu, N.Chen, W.Cao. *J. Alloys Compd.*, **513**, 539 (2012)
84. V.L.Chandraboss, J.Kamalakkannan, S.Senthilvelan. *Appl. Surf. Sci.*, **387**, 944 (2016)
85. T.Wang, X.Meng, G.Liu, K.Chang, P.Li, Q.Kang, L.Liu, M.Li, S.Ouyang, J.Ye. *J. Mater. Chem. A*, **3**, 9491 (2015)
86. Y.Gong, C.Fu, L.Ting, J.Chenu, Q.Zhao, C.Li. *Appl. Surf. Sci.*, **351**, 746 (2015)
87. X.F.Lei, X.X.Xue, H.Yang, C.Chen, X.Li, M.C.Niu, X.Y.Gao, Y.T.Yang. *Appl. Surf. Sci.*, **332**, 172 (2015)
88. L.Liu, F.Gao, H.Zhao, Y.Li. *Appl. Catal., B*, **134 – 135**, 349 (2013)
89. Q.Zhang, T.Gao, J.M.Andino, Y.Li. *Appl. Catal., B*, **123 – 124**, 257 (2012)
90. Slamet, H.W.Nasution, E.Purnama, S.Kosela, J.Gunlazuardi. *Catal. Commun.*, **6**, 313 (2005)
91. Y.Liu, S.Zhou, J. Li, Y.Wang, G.Jiang, Z.Zhao, B.Liu, X.Gong, A.Duan, J.Liu, Y.Wei, L.Zhang. *Appl. Catal., B*, **168 – 169**, 125 (2015)
92. M.Tahir, N.A.S.Amin. *Appl. Catal., B*, **162**, 98 (2015)
93. C.L.Muhich, J.Y.Westcott, T.Fuerst, A.W.Weimer, C.B.Musgrave. *J. Phys. Chem. C*, **118**, 27415 (2014)
94. H.Li, Y.Hao, H.Lu, L.Liang, Y.Wang, J.Qiu, X.Shi, Y.Wang, J.Yao. *Appl. Surf. Sci.*, **344**, 112 (2015)
95. O.Ola, M.M.Maroto-Valer. *J. Photochem. Photobiol., C*, **24**, 16 (2015)
96. M.Behpour, V.Atouf. *Appl. Surf. Sci.*, **258**, 6595 (2012)
97. R.Asahi, T.Morikawa, H.Irie, T.Ohwaki. *Chem. Rev.*, **114**, 9824 (2014)
98. J.Yu, P.Zhou, Q.Li. *Phys. Chem. Chem. Phys.*, **15**, 12040 (2013)
99. Z.Zhao, J.Fan, J.Wang, R.Li. *Catal. Commun.*, **21**, 32 (2012)
100. Z.Zhang, Z.Huang, X.Cheng, Q.Wang, Y.Chen, P.Dong, X.Zhang. *Appl. Surf. Sci.*, **355**, 45 (2015)
101. C.Feng, Y.Pang, Y.Wang, M.Sun, C.Zhang, L.Zhang, Y.Zhou, D.Li. *Appl. Surf. Sci.*, **376**, 188 (2016)
102. P.Pathak, M.J.Meziani, L.Castillo, Y.P.Sun. *Green Chem.*, **7**, 667 (2005)
103. B.Fang, A.Bonakdarpour, K.Reilly, Y.Xing, F.Taghipour, D.P.Wilkinson. *ACS Appl. Mater. Interfaces*, **6**, 15488 (2014)
104. B.Ofuonye, J.Lee, M.Yan, C.Sun, J.M.Zuo, I.Adesida. *Semicond. Sci. Technol.*, **29**, (2014)
105. R.Steim, F.R.Kogler, C.J.Brabec. *J. Mater. Chem.*, **20**, 2499 (2010)
106. X.Feng, J.D.Sloppy, T.J.Latempa, M.Paulose, S.Komarneni, N.Bao, C.A.Grimes. *J. Mater. Chem.*, **21**, 13429 (2011)
107. Y.Liu, C.Miao, P.Yang, Y.He, J.Feng, D.Li. *Appl. Catal., B*, **244**, 919 (2019)
108. W.N.Wang, W.J.An, B.Ramalingam, S.Mukherjee, D.M.Niedzwiedzki, S.Gangopadhyay, P.Biswas. *J. Am. Chem. Soc.*, **134**, 11276 (2012)
109. X.Zhang, Y.L.Chen, R.S.Liu, D.P.Tsai. *Reports Prog. Phys.*, **76**, (2013)
110. K.Awazu, M.Fujimaki, C.Rockstuhl, J.Tominaga, H.Murakami, Y.Ohki, N.Yoshida, T.Watanabe. *J. Am. Chem. Soc.*, **130**, 1676 (2008)
111. P.Wang, B.Huang, X.Zhang, X.Qin, H.Jin, Y.Dai, Z.Wang, J.Wei, J.Zhan, S.Wang, J.Wang, M.H.Whangbo. *Chem. – Eur. J.*, **15**, 1821 (2009)
112. K.Kimura, S.I.Naya, Y.Jin-Nouchi, H.Tada. *J. Phys. Chem. C*, **116**, 7111 (2012)
113. M.Rycenga, C.M.Cobley, J.Zeng, W.Li, C.H.Moran, Q.Zhang, D.Qin, Y.Xia. *Chem. Rev.*, **111**, 3669 (2011)
114. C.Clavero. *Nat. Photonics*, **8**, 95 (2014)
115. W.Hou, W.H.Hung, P.Pavaskar, A.Goeppert, M.Aykol, S.B.Cronin. *ACS Catal.*, **1**, 929 (2011)
116. W.Tu, Y.Zhou, H.Li, P.Li, Z.Zou. *Nanoscale*, **7**, 14232 (2015)
117. Y.Sato, S.I.Naya, H.Tada. *APL Mater.*, **3**, 104502 (2015)
118. S.Feng, M.Wang, Y.Zhou, P.Li, W.Tu, Z.Zou. *APL Mater.*, **3**, 104416 (2015)
119. J.Jiao, Y.Wei, Z.Zhao, W.Zhong, J.Liu, J.Li, A.Duan, G.Jiang. *Catal. Today*, **258**, 319 (2015)
120. F.Wang, Y.Zhou, P.Li, L.Kuai, Z.Zou. *Cuihua Xuebao/ Chinese J. Catal.*, **37**, 863 (2016)
121. W.Pipornpong, R.Wanbayor, V.Ruangpornvisuti. *Appl. Surf. Sci.*, **257**, 10322 (2011)
122. X.Meng, S.Ouyang, T.Kako, P.Li, Q.Yu, T.Wang, J.Ye. *Chem. Commun.*, **50**, 11517 (2014)
123. L.Liu, C.Zhao, H.Zhao, D.Pitts, Y.Li. *Chem. Commun.*, **49**, 3664 (2013)
124. Y.Liao, S.W.Cao, Y.Yuan, Q.Gu, Z.Zhang, C.Xue. *Chem. – Eur. J.*, **20**, 10220 (2014)
125. A.D.Ebner, M.L.Gray, N.G.Chisholm, Q.T.Black, D.D.Mumford, M.A.Nicholson, J.A.Ritter. *Ind. Eng. Chem. Res.*, **50**, 5634 (2011)
126. Q.Huang, J.Yu, S.Cao, C.Cui, B.Cheng. *Appl. Surf. Sci.*, **358**, 350 (2015)
127. L.J.Guo, Y.J.Wang, T.He. *Chem. Rec.*, 1918 (2016)
128. C.Tang, W.Hou, E.Liu, X.Hu, J.Fan. *J. Lumin.*, **154**, 305 (2014)
129. G.Xi, S.Ouyang, J.Ye. *Chem. – Eur. J.*, **17**, 9057 (2011)
130. K.Y.Lee, K.Sato, A.R.Mohamed. *Mater. Lett.*, **163**, 240 (2016)
131. Y.Zhao, X.Huang, X.Tan, T.Yu, X.Li, L.Yang, S.Wang. *Appl. Surf. Sci.*, **365**, 209 (2016)
132. B.Sun, G.Zhou, T.Gao, H.Zhang, H.Yu. *Appl. Surf. Sci.*, **364**, 322 (2016)

133. H.Okumura, S.Endo, S.Joonwichien, E.Yamasue, K.N.Ishihara. *Catal. Today*, **258**, 634 (2015)
134. L.Li, P.A.Salvador, G.S.Rohrer. *Nanoscale*, **6**, 24 (2014)
135. J.Lin, J.Shen, R.Wang, J.Cui, W.Zhou, P.Hu, D.Liu, H.Liu, J.Wang, R.I.Boughton, Y.Yue. *J. Mater. Chem.*, **21**, 5106 (2011)
136. J.Zhang, Y.Hu, X.Jiang, S.Chen, S.Meng, X.Fu. *J. Hazard. Mater.*, **280**, 713 (2014)
137. G.Liu, L.Wang, H.G.Yang, H.-M.Cheng, G.Q.Lu. *J. Mater. Chem.*, **20**, 831 (2010)
138. Y.Liu, G.Ji, M.A.Dastageer, L.Zhu, J. Wang, B.Zhang, X.Chang, M.A.Gondal. *RSC Adv.*, **4**, 56961 (2014)
139. P.Zhou, J.Yu, M.Jaroniec. *Adv. Mater.*, **26**, 4920 (2014)
140. L.Kuai, Y.Zhou, W.Tu, P.Li, H.Li, Q.Xu, L.Tang, X.Wang, M.Xiao, Z.Zou. *RSC Adv.*, **5**, 88409 (2015)
141. J.Yu, S.Wang, J.Low, W.Xiao. *Phys. Chem. Chem. Phys.*, **15**, 16883 (2013)
142. M.Dahl, Y.Liu, Y.Yin. *Chem. Rev.*, **114**, 9853 (2014)
143. J.Yu, J.Low, W.Xiao, P.Zhou, M.Jaroniec. *J. Am. Chem. Soc.*, **136**, 8839 (2014)
144. S.Gao, W.Wang, Y.Ni, C.Lu, Z.Xu. *J. Alloys Compd.*, **647**, 981 (2015)
145. L.Yang, M.Gao, B.Dai, X.Guo, Z.Liu, B.Peng. *Appl. Surf. Sci.*, **386**, 337 (2016)
146. S.Demirci, T.Dikici, M.Yurddaskal, S.Gultekin, M.Toparli, E.Celik. *Appl. Surf. Sci.*, **390**, 591 (2016)
147. G.Song, F.Xin, J.Chen, X.Yin. *Appl. Catal., A*, **473**, 90 (2014)
148. D.Xiong, H.Chang, Q.Zhang, S.Tian, B.Liu, X.Zhao. *Appl. Surf. Sci.*, **347**, 747 (2015)
149. Y.Li, W.Zhang, X.Shen, P.Peng, L.Xiong, Y.Yu. *Cuihua Xuebao/Chinese J. Catal.*, **36**, 2229 (2015)
150. M.E.Aguirre, R.Zhou, A.J.Eugene, M.I.Guzman, M.A.Grela. *Appl. Catal., B*, **217**, 485 (2017)
151. H.Wang, L.Zhang, Z.Chen, J.Hu, S.Li, Z.Wang, J.Liu, X.Wang. *Chem. Soc. Rev.*, **43**, 5234 (2014)
152. S.J.A.Moniz, S.A.Shevlin, D.J. Martin, Z.X.Guo, J.Tang. *Energy Environ. Sci.*, **8**, 731 (2015)
153. J.Chen, S.Lin, G.Yan, L.Yang, X.Chen. *Catal. Commun.*, **9**, 65 (2008)
154. D.V.Markovskaya, M.N.Lyulyukin, A.V.Zhurenok, E.A.Kozlova. *Kinet. Catal.*, **62**, 488 (2021)
155. X.Li, H.Liu, D.Luo, J.Li, Y.Huang, H.Li, Y.Fang, Y.Xu, L.Zhu. *Chem. Eng. J.*, **180**, 151 (2012)
156. A.Ahmad Beigi, S.Fatemi, Z.Salehi. *J. CO_2 Util.*, **7**, 23 (2014)
157. M.Inagaki. *Carbon NY*, **50**, 3247 (2012)
158. R.Leary, A.Westwood. *Carbon NY*, **49**, 741 (2011)
159. M.Q.Yang, N.Zhang, Y.J.Xu. *ACS Appl. Mater. Interfaces*, **5**, 1156 (2013)
160. E.Liu, L.Kang, F.Wu, T.Sun, X.Hu, Y.Yang, H.Liu, J.Fan. *Plasmonics*, **9**, 61 (2014)
161. Y.Wang, Q.Lai, Y.He, M.Fan. *Catal. Commun.*, **108**, 98 (2018)
162. Y.Wei, J.Jiao, Z.Zhao, J.Liu, J.Li, G.Jiang, Y.Wang, A.Duan. *Appl. Catal., B*, **179**, 422 (2015)
163. I.H.Tseng, J.C.S.Wu. *Catal. Today*, **97**, 113 (2004)
164. N.Singhal, A.Ali, A.Vorontsov, C.Pendem, U.Kumar. *Appl. Catal., A*, **523**, 107 (2016)
165. Q.Li, B.Guo, J.Yu, J.Ran, B.Zhang, H.Yan, J.R.Gong. *J. Am. Chem. Soc.*, **133**, 10878 (2011)
166. M.Liu, D.Jing, Z.Zhou, L.Guo. *Nat. Commun.*, **4**, 1 (2013)
167. S.Wang, X.Wang. *Appl. Catal., B*, **162**, 494 (2015)
168. X.Li, J.Chen, H.Li, J.Li, Y.Xu, Y.Liu, J.Zhou. *J. Nat. Gas Chem.*, **20**, 413 (2011)
169. L.Tang, L.Kuai, Y.Li, H.Li, Y.Zhou, Z.Zou. *Nanotechnology*, **29**, 064003 (2017)
170. E.A.Kozlova, M.N.Lyulyukin, D.V.Markovskaya, D.S.Selishchev, S.V.Cherepanova, D.V.Kozlov. *Photochem. Photobiol. Sci.*, **18**, 871 (2019)
171. E.A.Kozlova, A.Y.Kurenkova, V.S.Semeykina, E.V.Parkhomchuk, S.V.Cherepanova, E.Y.Gerasimov, A.A.Saraev, V.V.Kaichev, V.N.Parmon. *ChemCatChem*, **7**, 4108 (2015)
172. X.Meng, G.Zuo, P.Zong, H.Pang, J.Ren, X.Zeng, S.Liu, Y.Shen, W.Zhou, J.Ye. *Appl. Catal., B*, **237**, 68 (2018)
173. E.A.Kozlova, M.N.Lyulyukin, D.V.Markovskaya, A.V.Bukhtiyarov, I.P.Prosvirin, S.V.Cherepanova, D.V.Kozlov. *Top. Catal.*, **63**, 121 (2020)
174. M.N.Lyulyukin, A.Y.Kurenkova, A.V.Bukhtiyarov, E.A.Kozlova. *Mendeleev Commun.*, **30**, 192 (2020)
175. D.V.Markovskaya, E.A.Kozlova, S.V.Cherepanova, P.A.Kolinko, E.Y.Gerasimov, V.N.Parmon. *ChemPhotoChem*, **1**, 575 (2017)
176. Y.-Y.Li, Z.-H.Wei, J.-B.Fan, Z.-J.Li, H.-C.Yao. *Appl. Surf. Sci.*, **483**, 442 (2019)
177. C.Bie, B.Zhu, F.Xu, L.Zhang, J.Yu. *Adv. Mater.*, **31**, 1902868 (2019)
178. S.Wu, H.Pang, W.Zhou, B.Yang, X.Meng, X.Qiu, G.Chen, L.Zhang, S.Wang, X.Liu, R.Ma, J.Ye, N.Zhang. *Nanoscale*, **12**, 8693 (2020)
179. X.-F.Xie, X.-Y.Dao, F.Guo, X.-Y.Zhang, F.-M.Wang, W.-Y.Sun. *ChemistrySelect*, **5**, 4001 (2020)
180. K.Li, B.Peng, T.Peng. *ACS Catal.*, **6**, 7485 (2016)
181. S.Ye, R.Wang, M.-Z.Wu, Y.-P.Yuan. *Appl. Surf. Sci.*, **358**, 15 (2015)
182. W.-J.Ong, L.-L.Tan, Y.H.Ng, S.-T.Yong, S.-P.Chai. *Chem. Rev.*, **116**, 7159 (2016)
183. Y.Huang, K.Wang, T.Guo, J.Li, X.Wu, G.Zhang. *Appl. Catal., B*, **277**, 119232 (2020)
184. A.Raza, H.Shen, A.A.Haidry. *Appl. Catal. B Environ.*, **277**, 119239 (2020)
185. N.Li, X.Liu, J.Zhou, W.Chen, M.Liu. *Chem. Eng. J.*, **399**, 125782 (2020)
186. H.Qin, R.-t.Guo, X.-y.Liu, X.Shi, Z.-y.Wang, J.-y.Tang, W.-g.Pan. *Colloids Surf. A: Physicochem. Eng. Asp.*, **600**, 124912 (2020)
187. G.Zhou, J.Yang, X.Zhu, Q.Li, Q.Yu, W.El-alami, C.Wang, Y.She, J.Qian, H.Xu, H.Li. *J. Energy Chem.*, **49**, 89 (2020)
188. H.Zhang, Y.Tang, Z.Liu, Z.Zhu, X.Tang, Y.Wang. *Chem. Phys. Lett.*, **751**, 137467 (2020)
189. C.Yang, Q.Tan, Q.Li, J.Zhou, J.Fan, B.Li, J.Sun, K.Lv. *Appl. Catal., B*, **268**, 118738 (2020)
190. J.He, P.Lv, J.Zhu, H.Li. *RSC Adv.*, **10**, 22460 (2020)
191. W.Ma, N.Wang, Y.Guo, L.Yang, M.Lv, X.Tang, S.Li. *Chem. Eng. J.*, **388**, 124288 (2020)
192. Z.Sun, W.Fang, L.Zhao, H.Wang. *Appl. Surf. Sci.*, **504**, 144347 (2020)
193. H.Guo, J.Ding, S.Wan, Y.Wang, Q.Zhong. *Appl. Surf. Sci.*, **528**, 146943 (2020)
194. Q.Li, Z.Sun, H.Wang, Z.Wu. *J. CO_2 Util.*, **28**, 126 (2018)
195. N.Kolobov, M.G.Goesten, J.Gascon. *Angew. Chem., Int. Ed.*, anie. 202106342 (2021)
196. R.R.Ikreedeegh, M.Tahir. *J. CO_2 Util.*, **43**, 101381 (2021)

197. Y.Jiang, Y.Yu, X.Zhang, M.Weinert, X.Song, J.Ai, L.Han, H.Fei. *Angew. Chem., Int. Ed.*, (2021); https://doi.org/10.1002/anie.202105420
198. A.Perazio, G.Lowe, R.Gobetto, J.Bonin, M.Robert. *Coord. Chem. Rev.*, **443**, 214018 (2021)
199. Xiaopeng Li, Li Wang, Wei Su, Yi Xing. *New J. Chem.*, **45**, 2315 (2021)
200. M.Tahir, A.Ali Khan, S.Tasleem, R.Mansoor, W.K.Fan. *Energy Fuels*, **35**, 10374 (2021)
201. Sourav Rej, Matteo Bisetto, Alberto Naldoni, Paolo Fornasiero. *J. Mater. Chem. A*, **9**, 5915 (2021)
202. J.Mao, K.Li, T.Peng. *Catal. Sci. Technol.*, **3**, 2481 (2013)
203. R.E.Blankenship, D.M.Tiede, J. Barber, G.W.Brudvig, G.Fleming, M.Ghirardi, M.R.Gunner, W.Junge, D.M.Kramer, A.Melis, T.A.Moore, C.C.Moser, D.G.Nocera, A.J.Nozik, D.R.Ort, W.W.Parson, R.C.Prince, R.T.Sayre. *Science*, **332**, 805 (2011)
204. H.P.Jia, E.A.Quadrelli. *Chem. Soc. Rev.*, **43**, 547 (2014)
205. H.Liu. *Cuihua Xuebao/Chinese J. Catal.*, **35**, 1619 (2014)
206. G.Ertl, D.Prigge, R.Schloegl, M.Weiss. *J. Catal.*, **79**, 359 (1983)
207. G.Ertl. *J. Vac. Sci. Technol., A*, **1**, 1247 (1983)
208. J.W.Erisman, M.A.Sutton, J.Galloway, Z.Klimont, W.Winiwarter. *Nat. Geosci.*, **1**, 636 (2008)
209. G.N.Schrauzer, T.D.Guth. *J. Am. Chem. Soc.*, **99**, 7189 (1977)
210. S.Sun, X.Li, W.Wang, L.Zhang, X.Sun. *Appl. Catal., B*, **200**, 323 (2017)
211. T.A.Bazhenova, A.E.Shilov. *Coord. Chem. Rev.*, **144**, 69 (1995)
212. C.J.M.Van Der Ham, M.T.M.Koper, D.G.H.Hetterscheid. *Chem. Soc. Rev.*, **43**, 5183 (2014)
213. X.Li, J.Yu, M.Jaroniec. *Chem. Soc. Rev.*, **45**, 2603 (2016)
214. S.Hoang, P.X.Gao. *Adv. Energy Mater.*, **6**, 1600683 (2016)
215. J.Low, J.Yu, M.Jaroniec, S.Wageh, A.A.Al-Ghamdi. *Adv. Mater.*, **29**, 1601694 (2017)
216. H.Li, Y.Zhou, W.Tu, J.Ye, Z.Zou. *Adv. Funct. Mater.*, **25**, 998 (2015)
217. F.K.Kessler, Y.Zheng, D.Schwarz, C.Merschjann, W.Schnick, X.Wang, M.J.Bojdys. *Nat. Rev. Mater.*, **2**, 17030 (2017)
218. V.N.Parmon. In *Termodinamika Neravnovesnykh Protsessov dlya Khimikov. S Prilozheniem k Khimicheskoi Kinetike, Katalizu, Materialovedeniyu i Biologii (Thermodynamics of Nonequilibrium Processes for Chemists. With Application to Chemical Kinetics, Catalysis, Materials Science and Biology)* (Dolgoprudnyi: ID Intellekt, 2015). P. 472
219. N.M.Bazhin, V.N.Parmon. In *Termodinamika dlya Khimikov. (Thermodynamics for Chemists)*. (Saint Petersburg: Lan', 2019). P. 744
220. L.M.Azofra, N.Li, D.R.Macfarlane, C.Sun. *Energy Environ. Sci.*, **9**, 2545 (2016)
221. H.Li, J. Shang, J.Shi, K.Zhao, L.Zhang. *Nanoscale*, **8**, 1986 (2016)
222. J.S.Anderson, J.Rittle, J.C.Peters. *Nature (London)*, **501**, 84 (2013)
223. M.A.Shipman, M.D.Symes. *Catal. Today*, **286**, 57 (2017)
224. S.Bourgeois, D.Diakite, M.Perdereau. *React. Solids*, **6**, 95 (1988)
225. H.Hirakawa, M.Hashimoto, Y.Shiraishi, T.Hirai. *J. Am. Chem. Soc.*, **139**, 10929 (2017)
226. M.Lashgari, P.Zeinalkhani. *Appl. Catal., A*, **529**, 91 (2017)
227. M.M.Khader, N.N.Lichtin, G.H.Vurens, M.Salmeron, G.A.Somorjai. *Langmuir*, **3**, 303 (1987)
228. C.J.H.Jacobsen, S.Dahl, B.G.S.Clausen, S.Bahn, A.Logadottir, J.K.Nørskov. *J. Am. Chem. Soc.*, **123**, 8404 (2001)
229. E.Endoh, J.K.Leland, A.J.Bard. *J. Phys. Chem.*, **90**, 6223 (1986)
230. W.Zhao, H.Xi, M.Zhang, Y.Li, J.Chen, J.Zhang, X.Zhu. *Chem. Commun.*, **51**, 4785 (2015)
231. S.Sun, Q.An, W.Wang, L.Zhang, J.Liu, W.A.Goddard. *J. Mater. Chem. A*, **5**, 201 (2017)
232. C.M.Janet, S.Navaladian, B.Viswanathan, T.K.Varadarajan, R.P.Viswanath. *J. Phys. Chem. C*, **114**, 2622 (2010)
233. J.Soria, J.C.Conesa, V.Augugliaro, L.Palmisano, M.Schiavello, A.Sclafani. *J. Phys. Chem.*, **95**, 274 (1991)
234. V.Augugliaro, F.D'Alba, L.Rizzuti, M.Schiavello, A.Sclafani. *Int. J. Hydrogen Energy*, **7**, 851 (1982)
235. D.Cordischi, N.Burriesci, F.D'Alba, M.Petrera, G.Polizzotti, M.Schiavello. *J. Solid State Chem.*, **56**, 182 (1985)
236. O.Rusina, A.Eremenko, G.Frank, H.P.Strunk, H.Kisch. *Angew. Chem., Int. Ed.*, **40**, 3993 (2001)
237. O.Rusina, O.Linnik, A.Eremenko, H.Kisch. *Chem. – Eur. J.*, **9**, 561 (2003)
238. T.Oshikiri, K.Ueno, H.Misawa. *Angew. Chem., Int. Ed.*, **53**, 9802 (2014)
239. T.Oshikiri, K.Ueno, H.Misawa. *Angew. Chem.*, **128**, 4010 (2016)
240. H.Miyama, N.Fujii, Y.Nagae. *Chem. Phys. Lett.*, **74**, 523 (1980)
241. K.A.Brown, D.F.Harris, M.B.Wilker, A.Rasmussen, N.Khadka, H.Hamby, S.Keable, G.Dukovic, J.W.Peters, L.C.Seefeldt, P.W.King. *Science*, **352**, 448 (2016)
242. L.Ye, C.Han, Z.Ma, Y.Leng, J.Li, X.Ji, D.Bi, H.Xie, Z.Huang. *Chem. Eng. J.*, **307**, 311 (2017)
243. H.Li, J. Shang, Z.Ai, L.Zhang. *J. Am. Chem. Soc.*, **137**, 6393 (2015)
244. S.Hu, X.Chen, Q.Li, Y.Zhao, W.Mao. *Catal. Sci. Technol.*, **6**, 5884 (2016)
245. Y.Cao, S.Hu, F.Li, Z.Fan, J.Bai, G.Lu, Q.Wang. *RSC Adv.*, **6**, 49862 (2016)
246. Q.Zhang, S.Hu, Z.Fan, D.Liu, Y.Zhao, H.Ma, F.Li. *Dalton Trans.*, **45**, 3497 (2016)
247. S.Hu, Y.Li, F.Li, Z.Fan, H.Ma, W.Li, X.Kang. *ACS Sustain. Chem. Eng.*, **4**, 2269 (2016)
248. S.Wu, J.S.Ross, G.Bin Liu, G.Aivazian, A.Jones, Z.Fei, W.Zhu, D.Xiao, W.Yao, D.Cobden, X.Xu. *Nat. Phys.*, **9**, 149 (2013)
249. K.F.Mak, K.He, J.Shan, T.F.Heinz. *Nat. Nanotechnol.*, **7**, 494 (2012)
250. E.A.A.Pogna, M.Marsili, D.De Fazio, S.Dal Conte, C.Manzoni, D.Sangalli, D.Yoon, A.Lombardo, A.C.Ferrari, A.Marini, G.Cerullo, D.Prezzi. *ACS Nano*, **10**, 1182 (2016)
251. S.Wu, C.Huang, G.Aivazian, J.S.Ross, D.H.Cobden, X.Xu. *ACS Nano*, **7**, 2768 (2013)
252. C.H.Lui, A.J.Frenzel, D.V.Pilon, Y.H.Lee, X.Ling, G.M.Akselrod, J.Kong, N.Gedik. *Phys. Rev. Lett.*, **113**, 1 (2014)
253. T.Spatzal, M.Aksoyoglu, L.Zhang, S.L.A.Andrade, E.Schleicher, S.Weber, D.C.Rees, O.Einsle. *Science*, **334**, 940 (2011)
254. H.Cheng, B.Huang, Y.Dai. *Nanoscale*, **6**, 2009 (2014)

255. X.Y.Kong, W.P.C.Lee, W.J.Ong, S.P.Chai, A.R.Mohamed. *ChemCatChem*, **8**, 3074 (2016)
256. W.L.Huang, Q.Zhu. *J. Comput. Chem.*, **30**, 183 (2009)
257. S.Wang, X.Hai, X.Ding, K.Chang, Y.Xiang, X.Meng, Z.Yang, H.Chen, J.Ye. *Adv. Mater.*, **29**, 1 (2017)
258. H.Li, J.Li, Z.Ai, F.Jia, L.Zhang. *Angew. Chem., Int. Ed.*, **57**, 122 (2018)
259. Y.Bai, L.Ye, T.Chen, L.Wang, X.Shi, X.Zhang, D.Chen. *ACS Appl. Mater. Interfaces*, **8**, 27661 (2016)
260. O.A.Ileperuma, K.Tennakone, W.D.D.P.Dissanayake. *Appl. Catal.*, **62**, L1 (1990)
261. K.T.Ranjit, T.K.Varadarajan, B.Viswanathan. *J. Photochem. Photobiol., A*, **96**, 181 (1996)
262. Q.-S.Li, K.Domen, S.Naito, T.Onishi, T.Kenzi. *Chem. Lett.*, **12**, 321 (1983)
263. H.Zeng, S.Terazono, T.Tanuma. *Catal. Commun.*, **59**, 40 (2015)
264. S.E.Braslavsky, A.M.Braun, A.E.Cassano, A.V.Emeline, M.I.Litter, L.Palmisano, V.N.Parmon, N.Serpone. *Pure Appl. Chem.*, **83**, 931 (2011)